Piccolo modulation of Synapsin1a dynamics regulates synaptic vesicle exocytosis

Sergio Leal-Ortiz,[1] Clarissa L. Waites,[1] Ryan Terry-Lorenzo,[1] Pedro Zamorano,[2] Eckart D. Gundelfinger,[3] and Craig C. Garner[1]

[1]Deptartment of Psychiatry and Behavioral Science, Nancy Pritzker Laboratory, Stanford University, Palo Alto, CA 94304
[2]Deptartment of Biochemistry, University of Antofagasta, Antofagasta, Chile
[3]Deptartment of Neurochemistry and Molecular Biology, Leibniz Institute for Neurobiology, Magdeburg D-39118, Germany

Active zones are specialized regions of the presynaptic plasma membrane designed for the efficient and repetitive release of neurotransmitter via synaptic vesicle (SV) exocytosis. Piccolo is a high molecular weight component of the active zone that is hypothesized to participate both in active zone formation and the scaffolding of key molecules involved in SV recycling. In this study, we use interference RNAs to eliminate Piccolo expression from cultured hippocampal neurons to assess its involvement in synapse formation and function. Our data show that Piccolo is not required for glutamatergic synapse formation but does influence presynaptic function by negatively regulating SV exocytosis. Mechanistically, this regulation appears to be calmodulin kinase II–dependent and mediated through the modulation of Synapsin1a dynamics. This function is not shared by the highly homologous protein Bassoon, which indicates that Piccolo has a unique role in coupling the mobilization of SVs in the reserve pool to events within the active zone.

Introduction

Presynaptic boutons are sophisticated compartments designed for the rapid, regulated release of neurotransmitter via synaptic vesicles (SVs). SVs release neurotransmitter at specialized sites called active zones (AZs; Schoch and Gundelfinger, 2006), which appear by electron microscopy as domains containing docked SVs intermingled with tufts of electron-dense material. These electron-dense tufts are thought to represent the cytoskeletal matrix assembled at the AZ (CAZ), which is comprised of a collection of multidomain scaffold proteins including ELKS (ERC/CAST), Liprin1α, RIMs, RIMBPs, Bassoon, and Piccolo. The CAZ has hypothesized roles in structurally defining the AZ, maintaining it in register with postsynaptic structures, regulating its size, and recruiting key molecules involved in SV exocytosis such as Munc13 and voltage-gated calcium channels (Garner et al., 2000; Schoch and Gundelfinger, 2006; Fejtova and Gundelfinger, 2006).

With the notable exceptions of RIMs and Munc13, our understanding of the roles played by individual CAZ proteins is very limited. In particular, the functions of the two largest CAZ proteins, Piccolo and Bassoon, have remained elusive because of their enormous sizes (>400 kD). Both are expressed very early during neuronal differentiation (Cases-Langhoff et al., 1996; Zhai et al., 2000) and are among the first proteins to arrive at newly forming synapses (Friedman et al., 2000; Zhai et al., 2000; Shapira et al., 2003), which implicates them in nascent synapse formation (Ziv and Garner, 2004; Waites et al., 2005). These multidomain proteins are composed of two N-terminal zinc finger motifs, three coiled-coiled regions and, in the case of Piccolo, a PDZ and two C2 domains (Fig. 1 A; tom Dieck et al., 1998; Wang et al., 1999; Fenster et al., 2000). Interacting partners include other core components of the CAZ (e.g., ELKs and Liprin) as well as proteins involved in the regulation of actin and SV dynamics, such as GIT1, Abp1, profilin, and PRA-1 (Wang et al., 1999; Fenster et al., 2000; Fenster et al., 2003; Kim et al., 2003; tom Dieck et al., 2005; Fejtova and Gundelfinger, 2006).

Studies of Bassoon knockout mice, in which photoreceptor ribbon synapses are grossly malformed (e.g., ribbons detached from the AZ), support a structural role for this protein (tom Dieck et al., 1998, 2005; Altrock et al., 2003). The loss of

S.L. Ortiz and C.L. Waites contributed equally to this paper.

Correspondence to C.C. Garner: cgarner@stanford.edu

Abbreviations used in this paper: ANOVA, analysis of variance; AZ, active zone; CaMKII, CaM-dependent kinase II; CAZ, cytoskeletal matrix assembled at the active zone; DIV, days in vitro; MAP2, microtubule-associated protein 2; Pr, probability of release; PSD, postsynaptic density; RRP, readily releasable pool; shRNA, short hairpin RNA; SV, synaptic vesicle; TRP, total recycling pool; VAMP2, vesicle-associated membrane protein 2.

The online version of this paper contains supplemental material.

The Rockefeller University Press $30.00
J. Cell Biol. Vol. 181 No. 5 831–846
www.jcb.org/cgi/doi/10.1083/jcb.200711167

Bassoon also reduces excitatory postsynaptic currents and increases the percentage of silent synapses in cultured hippocampal neurons; however, no overt structural defects are seen at these central nervous system synapses (Altrock et al., 2003). This milder phenotype could be caused by a more ancillary role for Bassoon at conventional synapses or by functional redundancy of another CAZ protein such as Piccolo. Addressing these issues using conventional knockout strategies has been hampered by the very large sizes of the genes encoding Piccolo and Bassoon (>350 kb) and the existence of alternatively spliced transcripts and uncharacterized 5′ promoter regions (Cases-Langhoff et al., 1996; tom Dieck et al., 1998; Winter et al., 1999; Fenster and Garner, 2002; Altrock et al., 2003). As a case in point, the Bassoon knockout mouse is not a genetic null but rather a deletion of two large central exons from the Bsn gene, leaving the N and C termini intact. Careful analysis of these mice has demonstrated that these domains, including the N-terminal Zinc finger motifs and C-terminal coiled-coil domain, are still expressed and synaptically localized, which suggests that the true phenotype of Bassoon loss could be masked by the continued expression of these fragments.

In the present study, we have overcome these limitations by using interference RNA to completely eliminate the expression of Piccolo in cultured hippocampal neurons. Our data reveal that although Piccolo is not essential for the formation of glutamatergic synapses, it does play a functional role in SV recycling. Specifically, synapses lacking Piccolo exhibit enhanced SV exocytosis rates, apparently caused by alterations in the activity-dependent dynamics of Synapsin1a at presynaptic boutons. These defects are not detected at synapses lacking Bassoon, which indicates that Piccolo has a specific role in coupling events at the AZ with the regulated recruitment of SVs from the reserve pool.

Results

Design of short hairpin RNAs (shRNAs) that selectively and efficiently knock down Piccolo

To eliminate the expression of Piccolo in developing neurons, we generated several shRNAs against sequences situated in the N terminus of Piccolo (Exon 1; Fig. 1 A; Fenster and Garner, 2002). This region has been shown to encode segments of the highest molecular weight Piccolo isoforms (~560 kD; Fig. 1 A; Fenster et al., 2000; Fenster and Garner, 2002) shown previously to localize to presynaptic AZs (Cases-Langhoff et al., 1996; Fenster et al., 2000; Zhai et al., 2000). After developing and testing two such shRNAs – Pclo6 and Pclo28 – in HEK cells, we assessed their efficacy in neurons using plasmid-based transfection (Fig. S1, available at http://www.jcb.org/cgi/content/full/jcb.200711167/DC1). Pclo28 was slightly more effective than Pclo6 at eliminating Piccolo expression, and was thus used for all further experiments presented in this paper. However, key experiments were repeated with Pclo6 to verify that the observed phenotypes were not caused by off-target effects (Fig. S2).

Given the low efficiency and potential overexpression associated with plasmid-based transfection, we next evaluated whether Pclo28 introduced via lentivirus would similarly eliminate Piccolo in cultured neurons. This was accomplished by subcloning both an EGFP-Synapsin1a reporter gene (for labeling presynaptic boutons expressing Pclo28; Fig. S1) and the H1-driven shRNA into the FUGW vector (Fig. 1 B; Lois et al., 2002) to create LV/EGFP-Synapsin or LV/EGFP-Synapsin/Pclo28. As an initial measure of knockdown efficacy, lysates from 14-d-in-vitro (DIV) hippocampal neurons superinfected with lentivirus, in order to ensure nearly 100% infectivity, were Western blotted and probed with antibodies against Piccolo and several other neuronal proteins (Fig. 1 C). We observed a dramatic and selective loss of Piccolo in lysates from cells infected with Pclo28 and no effect on the levels of β-tubulin, Synaptophysin, Bassoon, or EGFP-Synapsin1a (Fig. 1 C).

We next assessed whether lentiviral expression of Pclo28 reduced synaptic Piccolo. Hippocampal neurons infected with LV/EGFP-Synapsin or LV/EGFP-Synapsin/Pclo28 were immunostained after 14 DIV with antibodies against Piccolo and Bassoon. In control cells, EGFP-Synapsin exhibited a punctate pattern along microtubule-associated protein 2 (MAP2)-positive dendritic profiles (Fig. 1 D), with >90% of these puncta immunopositive for Piccolo (Fig. 1, D and F) or Bassoon (Fig. 1, E and G). In contrast, hippocampal cultures infected with LV/EGFP-Synapsin1a/Pclo28 exhibited a dramatic loss of Piccolo immunoreactivity at EGFP-Synapsin1a clusters, with <3% of clusters along dendritic profiles containing Piccolo (Fig. 1 F). Importantly, this shRNA had no effect on Bassoon protein levels or clustering at EGFP-Synapsin1a sites (Fig. 1, C, E, and G). Collectively, these data indicate that Pclo28 efficiently and selectively eliminates Piccolo from synapses.

Loss of Piccolo does not affect synapse formation or morphology

The appearance of axonal EGFP-Synapsin1a and Bassoon clusters in the absence of presynaptic Piccolo expression indicates that Piccolo is not necessary for synapse formation. To evaluate this hypothesis, we immunostained cultured neurons infected with either LV/EGFP-Synapsin1a or LV/EGFP-Synapsin1a/Pclo28 with antibodies against several key presynaptic (Synaptophysin, RIM1α, and Munc13-1) and postsynaptic (PSD-95 and NR1) proteins. As shown in Fig. 2, each exhibited a punctate pattern that reliably colocalized with EGFP-Synapsin-1a clusters along dendritic profiles, regardless of whether Piccolo was present (Fig. 2 A) or absent (Fig. 2 B). These data indicate that the loss of Piccolo does not disrupt the synaptic targeting of multiple key pre- and postsynaptic proteins.

To assess whether the loss of Piccolo affected synapse ultrastructure, we developed a strategy for visualizing boutons expressing Pclo28 by EM. This was achieved by replacing EGFP-Synapsin1a in the pZOff vector with vesicle-associated membrane protein 2 (VAMP2) tagged at its C terminus with HRP (VAMP2-HRP; Fig. 3 A). VAMP2 is an essential transmembrane component of SVs (Elferink et al., 1989; Sudhof et al., 1989), and in VAMP2-HRP, the C-terminal HRP is situated within the vesicle lumen. Upon reaction with hydrogen peroxide and DAB, HRP forms an electron-dense precipitate, enabling visualization of vesicles within boutons of neurons expressing

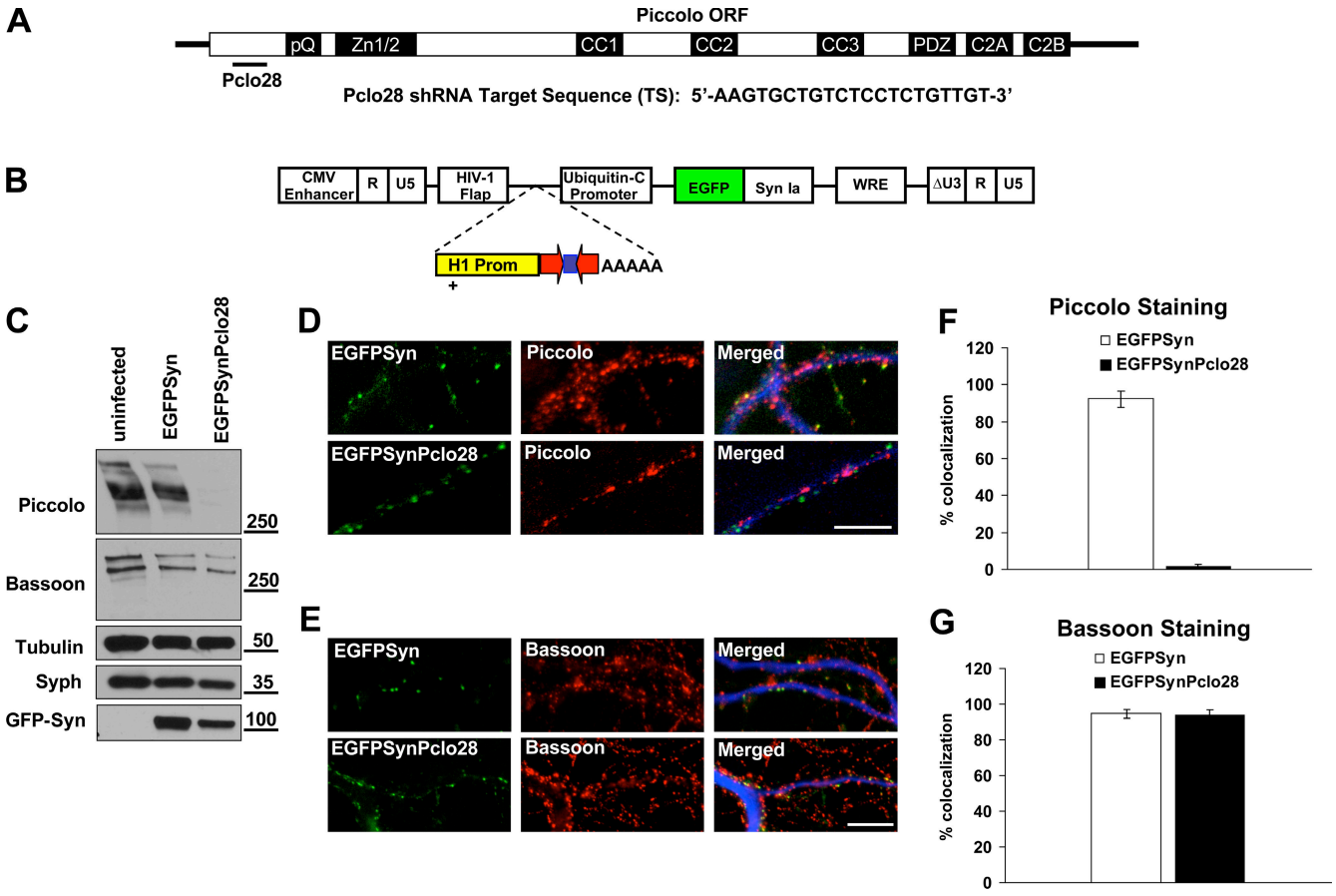

Figure 1. **Lentivirus mediated knockdown of Piccolo with interference RNAs.** (A) Schematic diagram of Piccolo, illustrating its multidomain structure (a polyglutamate [pQ] region, two double zinc finger domains [Zn1/2], three coiled-coil domains [CC1-3], a PDZ domain, and two C2 domains [C2A/B]) and the location and sequence of the shRNA (Pclo28) used in this study. (B) Schematic diagram of the lentiviral vector (FUGW H1) used to express shRNAs under control of the H1 promoter (H1 prom; yellow) and either EGFP or EGFP-Synapsin1a (Syn1a) under the ubiquitin-C promoter. (C) Western blots of cellular lysates from hippocampal neurons (uninfected or infected with LV/EGFP-Synapsin1a [EGFP-Syn] or LV/EGFP-Synapsin1a/Pclo28 [EGFPSynPclo28]) immunostained for Piccolo, Bassoon, tubulin, Synaptophysin (Syph), and GFP-Synapsin (GFP-Syn). Protein molecular weights are indicated on the right. (D and E) Hippocampal neurons infected with LV/EGFP-Synapsin1a (EGFPSyn) or LV/EGFP-Synapsin1a/Pclo28 (EGFPSynPclo28) and immunostained with antibodies against MAP2 (Merged, blue) and Piccolo (D, red) or Bassoon (E, red) after 14 DIV. Only a fraction of presynaptic boutons express EGFP-Synapsin1a/Pclo28; Piccolo immunoreactivity is from uninfected neurons. Bars, 10 µm. (F and G) Bar graphs showing percent colocalization of EGFP-Synapsin1a (EGFPSyn) puncta with either Piccolo (F) or Bassoon (G) puncta along dendritic profiles (n > 2,000 puncta per condition, five experiments). Error bars indicate SEM.

pZOff/VAMP2-HRP. To verify that VAMP2-HRP did not affect Piccolo down-regulation, cultures expressing pZOff/VAMP2-HRP or pZOff/VAMP2-HRP/Pclo28 were immunostained with antibodies against Piccolo and HRP at 6 DIV (Fig. 3 B). Under these conditions, Piccolo immunoreactivity was detected in the axons of untransfected neurons or those expressing VAMP2-HRP alone but not in axons of neurons expressing Pclo28. These data indicate that Pclo28 shRNA was not hampered by coexpression of VAMP2-HRP.

To visualize synapses, hippocampal neurons electroporated at the time of plating with pZOff/VAMP2-HRP or pZOff/VAMP2-HRP/Pclo28 were fixed and processed for EM at 14 DIV. In both cases, presynaptic boutons expressing VAMP2-HRP were readily identified based on the presence of electron-dense SVs (Fig. 3 D). These labeled SVs were easily distinguishable from both unlabeled SVs and the 80-nm dense core vesicles hypothesized to carry Piccolo and Bassoon to nascent synapses (Figs. 3 C and S3, available at http://www.jcb.org/cgi/content/full/jcb.200711167/DC1; Zhai et al., 2001). Qualitatively, no gross morphological differences were detected between unlabeled synapses, those expressing only VAMP2-HRP, and those expressing VAMP2-HRP/Pclo28 (Fig. 3, E and F). Furthermore, when synapses were carefully quantified for bouton area, AZ/postsynaptic density (PSD) length, docked SVs/AZ length, and SV density (number of vesicles per bouton area), no morphological differences were found (Table I). These data strongly suggest that Piccolo is not essential for the structural assembly of excitatory asymmetrical synapses.

Synapses lacking Piccolo exhibit faster rates of SV exocytosis

Although synapses still form in the absence of Piccolo, its large size and multiple binding partners suggest that it may be functionally important for SV recycling. We thus used the styryl FM dyes (Cochilla et al., 1999) to analyze presynaptic function. We first examined whether boutons lacking Piccolo were presynaptically active. This was accomplished by labeling the total recycling pool (TRP) of vesicles with FM4-64 (90 mM

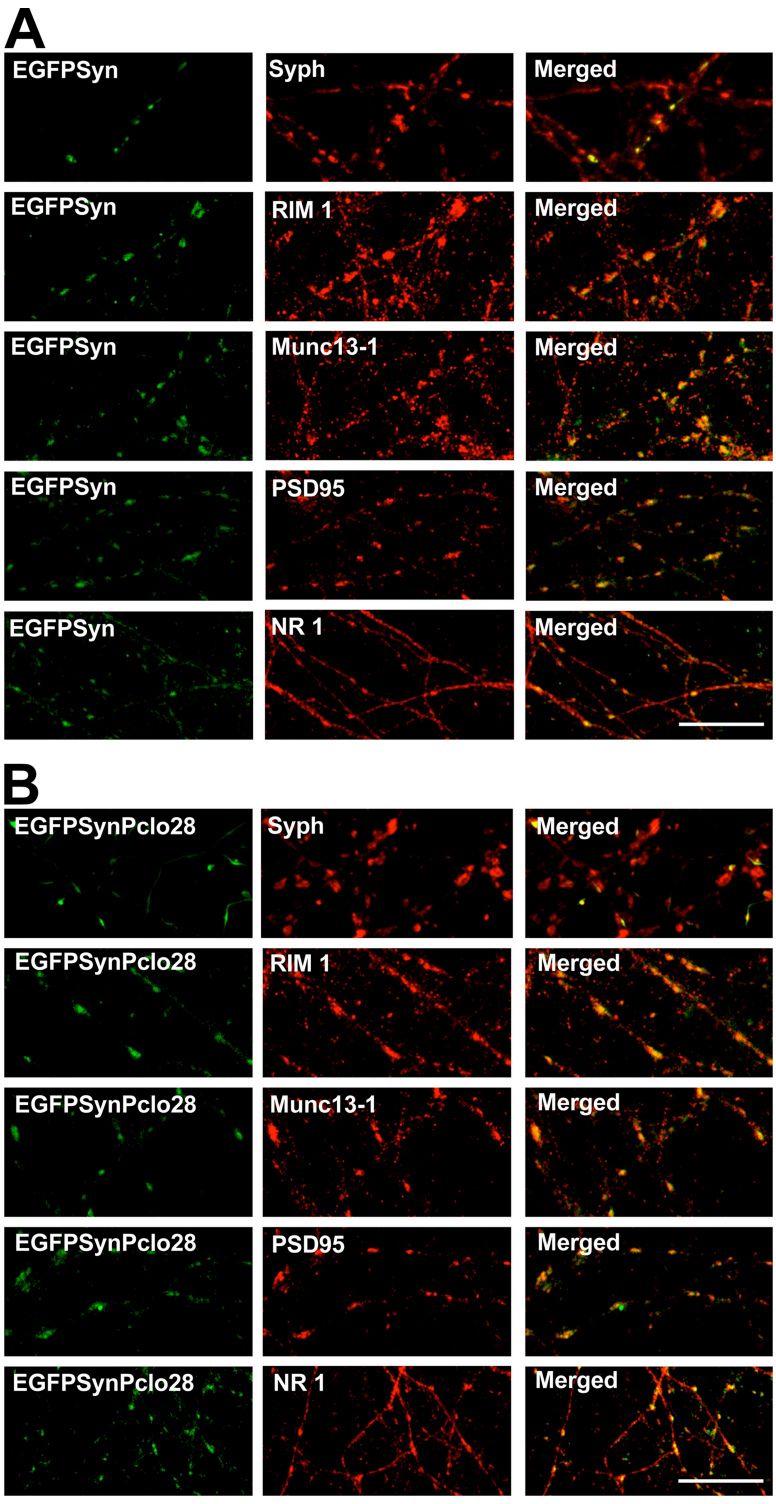

Figure 2. **Piccolo is not essential for the clustering of key pre- and postsynaptic proteins.** Hippocampal neurons infected with LV/EGFP-Synapsin1a (EGFP-Syn; A) or LV/EGFP-Synapsin1a/Pclo28 (EGFPSynPclo28; B) and immunostained with antibodies against Synaptophysin (Syph), RIM1, Munc13-1, PSD-95, or NR1 subunits of the NMDA receptor after 14 DIV. Shown are EGFP-Synapsin1a (green) puncta along dendrites (not depicted) that colocalize (Merged) with each pre- or postsynaptic protein (red). Bars, 10 µm.

KCl for 60 s; Pyle et al., 2000) in neuronal cultures infected with either LV/EGFP-Synapsin1a or LV/EGFP-Synapsin1a/Pclo28. At boutons with (EGFPSyn) or without (EGFPSynPclo28) Piccolo, >80% of EGFP-Synapsin1a clusters colocalized with FM4-64 puncta (Fig. 4, A and B). These data indicated that synapses lacking Piccolo were indeed presynaptically functional and no more likely to be silent than control boutons. We next compared the total FM fluorescence intensity at boutons containing or lacking Piccolo to determine the relative sizes of the TRP. No difference was observed in the mean intensity of FM4-64 fluorescence (Fig. 4 C), which indicates that TRP size was unaffected by the absence of Piccolo. To evaluate whether the loss of Piccolo led to changes in SV exocytosis, we compared the destaining kinetics of the TRP using both 10- and 5-Hz electrical stimulation (Fig. 4, D and E). Intriguingly, boutons lacking Piccolo destained more quickly than those expressing only EGFP-Synapsin1a (two-way analysis of variance [ANOVA]; $P < 0.0001$ for both conditions;

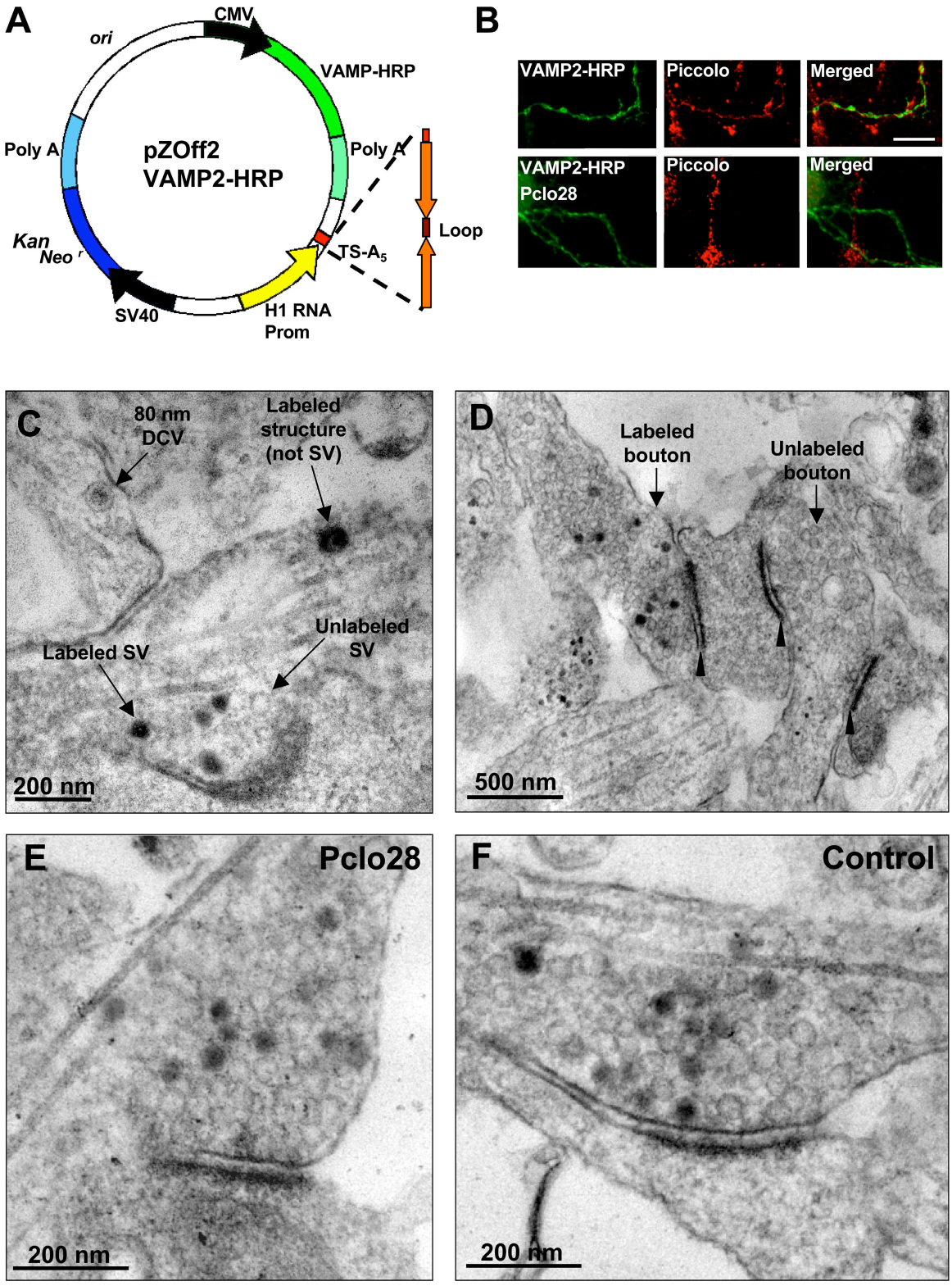

Figure 3. **Loss of Piccolo does not affect synapse ultrastructure.** (A) Schematic diagram of the pZOff/VAMP2-HRP vector used to express VAMP2-HRP with or without Pclo28 shRNA. (B) Hippocampal neurons electroporated at the time of plating with pZOff/VAMP2-HRP or pZOff/VAMP2-HRP/Pclo28 and immunostained at 6 DIV with HRP (green) and Piccolo (red) antibodies. Note the lack of Piccolo immunoreactivity in Pclo28-expressing axons. (C) Transmission EM micrograph of a VAMP2-HRP–positive bouton containing both clear-centered (unlabeled SV) and dark-centered SVs (labeled SV). HRP-labeled vesicles are easily distinguished from 80-nm DCVs and other labeled structures. (D) Synaptic boutons from VAMP2-HRP–expressing (labeled bouton) and untransfected (unlabeled bouton) neurons. Arrowheads denote synaptic junctions, identified based on electron-dense PSDs. (E) An excitatory synapse formed between a pZOff/VAMP2-HRP/Pclo28 (Pclo28)-transfected presynaptic bouton and a postsynaptic spine. (F) An excitatory synapse formed between a pZOff/VAMP2-HRP (control) transfected presynaptic bouton and a postsynaptic spine.

Table I. **Quantitative ultrastructural analysis of synapses with or without Pclo28**

Parameter	Control	+Pclo28
AZ length (nm)	0.258 ± 0.142	0.229 ± 0.102
Docked SVs/AV length (*n*/μm)	13.87 ± 6.26	14.29 ± 5.30
SV density (*n*/μm^2)	163.8 ± 58.36	169.0 ± 49.02
Percentage of SVs labeled	20.4 ± 12.5%	24.5 ± 14.8%

All data are from boutons with at least two clearly labeled synaptic vesicles opposed to a distinct synaptic junction. All parameters were measured by an observer blind to phenotype. *n* = 64 boutons with 66 active zones for control and 53 boutons with 55 active zones for +Pclo28. Data are shown ± standard deviation. *t* tests revealed no significant differences, with no $P < 0.05$.

Fig. 4, D and E), which indicates that Piccolo is a negative regulator of SV exocytosis.

Piccolo could regulate SV exocytosis by influencing vesicle docking and/or fusion with the AZ plasma membrane or by controlling SV translocation from the reserve to readily releasable pool (RRP). To explore possible changes in SV docking and/or fusion, we evaluated whether the size of the RRP of SVs or the release probability (Pr) were modified in the absence of Piccolo (Fig. 4, F and G). The former represents the subpopulation of SVs that are docked at the AZ plasma membrane and poised to undergo fusion with the arrival of an action potential, whereas the latter is a measure of the probability that SVs in the RRP will undergo fusion. Two methods were used to estimate RRP size: one using hypertonic sucrose (500 mM, ∼800 mOsm) and the other using a weak electrical stimulus (2 Hz for 30 s; Pyle et al., 2000). Under both conditions, we found no significant difference in RRP size between wild-type synapses and those lacking Piccolo (*t* test, $P > 0.5$; Fig. 4 F).

To determine Pr, we measured the destaining kinetics of boutons under conditions that stimulate RRP release, as described previously (Ryan et al., 1993; Pyle et al., 2000; Mozhayeva et al., 2002; Sankaranarayanan et al., 2003). Again, we found no significant difference in release probability between wild-type boutons and those lacking Piccolo (*t* test, $P > 0.5$; Fig. 4 G). Collectively, these data indicated that the increased SV exocytosis rates observed at 5 and 10 Hz were not caused by increased RRP size or Pr.

Piccolo modulates the dispersion kinetics of Synapsin1a

Based on the RRP experiments, we concluded that Piccolo's negative regulation of SV exocytosis was unlikely to occur at the level of SV priming or fusion, as described for RIM1α and Munc13 (Augustin et al., 1999; Schoch et al., 2002; Weimer and Richmond, 2005; Gracheva et al., 2006; Weimer et al., 2006), but rather at an earlier step, such as translocation of SVs from the reserve pool to the RRP. To date, the only protein that has been implicated in regulating SV translocation is the SV-associated phosphoprotein Synapsin (De Camilli et al., 1990; Greengard et al., 1993; Ryan et al., 1996; Chi et al., 2003). Mechanistically, Synapsin is hypothesized to mediate the clustering and retention of SVs within boutons via its ability to cross-bridge and tether them to the presynaptic actin/spectrin cytoskeleton (Greengard et al., 1993; Ceccaldi et al., 1995). Activity-dependent phosphorylation/dephosphorylation of Synapsin by CaM-dependent kinase II (CaMKII), protein kinase A, MAPK, and protein phosphatases 2A and 2B appears to regulate the exocytosis kinetics of SVs, presumably by regulating Synapsin binding to SVs and/or the actin cytoskeleton (Greengard et al., 1993; Ryan et al., 1993; Jovanovic et al., 2000, 2001; Pyle et al., 2000; Mozhayeva et al., 2002; Chi et al., 2003; Sankaranarayanan et al., 2003). Importantly, Synapsin has also been shown to undergo an activity-dependent dispersion away from presynaptic boutons (Chi et al., 2001), and the rate of dispersion is linked to its phosphorylation state (Chi et al., 2001, 2003). However, the precise relationship between Synapsin phosphorylation, dispersion, and SV exocytosis appears complex and has not been fully characterized.

To explore whether the loss of Piccolo impacts SV translocation via alterations in the properties of Synapsin, we evaluated whether the association and/or dispersion kinetics of Synapsin1a within presynaptic boutons were altered. Here, we took advantage of the fact that our shRNA expression vector contained EGFP-Synapsin1a. Initially, we used antibodies against Synapsin to verify that the lentiviral system did not lead to a gross overexpression of Synapsin at individual boutons. Surprisingly, we found no increase in Synapsin immunostaining at boutons expressing EGFP-Synapsin1a (Fig. 5 A), which indicates that endogenous Synapsin expression is downregulated in the presence of EGFP-Synapsin to maintain similar total levels per bouton. Next, we quantified and compared the synaptic levels of EGFP-Synapsin1a in boutons of control neurons and those expressing Pclo28. We found no discernable differences in fluorescence intensity when cultures were fixed with 4% paraformaldehyde (Fig. 5 B). However, when cultures were fixed with methanol, which extracts soluble proteins, we observed a significant decrease (*t* test, $P < 0.0001$) in the intensity of EGFP-Synapsin1a at boutons lacking Piccolo (Fig. 5 B). This suggested that EGFP-Synapsin1a was not as tightly associated with SVs and/or actin-related structures in the absence of Piccolo but rather was shifted into a more soluble fraction. This concept was supported by FRAP experiments designed to monitor the steady-state exchange kinetics of EGFP-Synapsin1a fluorescence at individual boutons (Fig. 5, C and D). Again, EGFP-Synapsin1a fluorescence recovered more quickly at boutons lacking Piccolo (τ_{fast} = 1.2 min and τ_{slow} = 11.9 min vs. τ_{fast} = 2.2 min and τ_{slow} = 33.7 min for control boutons; two-way ANOVA, $P < 0.0001$; Fig. 5 D), which indicates that mechanisms regulating the association of Synapsin1a with SVs and/or the actin/spectrin cytoskeleton were altered in the absence of Piccolo.

To assess whether the faster exchange kinetics of EGFP-Synapsin1a in the absence of Piccolo were caused by decreased presynaptic stability and/or association of SVs with synapses, we also examined the turnover rates of SV2, an SV integral membrane protein, in the presence and absence of Piccolo. Here, an N-terminally EGFP-tagged SV2 was subcloned into our lentiviral vectors in place of EGFP-Synapsin1a. Like EGFP-Synapsin1a, EGFP-SV2 reliably labeled presynaptic boutons, exhibiting a high degree of colocalization with FM4-64 (Fig. S4, available at

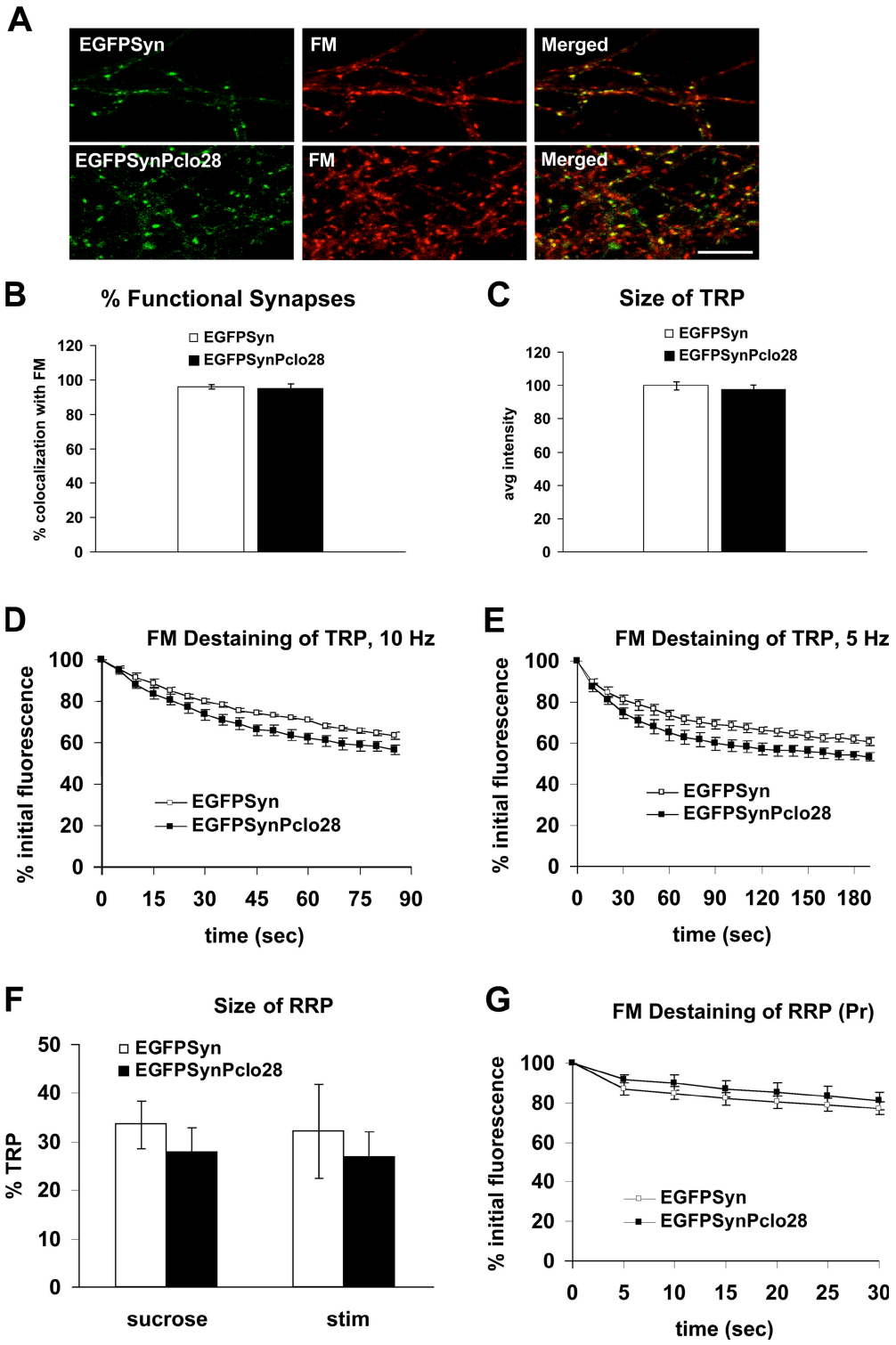

Figure 4. **Synapses lacking Piccolo have enhanced rates of SV exocytosis.** (A) Images of 14 DIV hippocampal neurons infected with LV/EGFP-Synapsin1a (EGFPSyn, green) or LV/EGFP-Synapsin1a/Pclo28 (EGPFSynPclo28, green) and loaded with FM4-64 (FM, red) with 90 mM K+. Note the high degree of match between EGFP-Synapsin1a and FM4-64 in both merged images. Bar, 10 µm. (B) Bar graphs quantifying the percent colocalization between EGFP-Synapsin and FM4-64 puncta in control cultures (EGFPSyn) or those lacking Piccolo (EGFPSynPclo28; $n > 800$ puncta per condition, two experiments). (C) Bar graph of FM4-64 fluorescence intensity at EGFP-Synapsin1a puncta comparing the relative sizes of the TRP of SVs at control synapses (EGFPSyn) and those lacking Piccolo (EGFPSynPclo28). FM intensity values at EGFPSyn-expressing boutons were normalized against those from neighboring uninfected cells to enable cross-coverslip comparison. Mean normalized FM intensity from control boutons was set to 100; that from Pclo28 boutons was ratioed against this value ($n > 800$ puncta, two experiments). (D and E) Destaining kinetics of the TRP at 10 Hz (D) and 5 Hz (E) comparing synapses with (EGFPSyn) and without (EGFPSynPclo28) Piccolo ($n = 5$ experiments per condition). (F) Bar graph comparing the size of the RRP of SVs in boutons with (EGFPSyn) or without (EGFPSynPclo28) Piccolo, as determined by either the application of 500 mM sucrose (left) or 2-Hz, 30-s stimulation (right). No significant differences were found (*t* test, $P > 0.5$). Sucrose experiments were performed twice for each condition and stimulation experiments three times. (G) Destaining kinetics of the RRP during 2-Hz, 30-s stimulation for control (EGFPSyn) boutons and those lacking Piccolo (EGFPSynPclo28; $n = 5$ experiments per condition). Error bars indicate SEM.

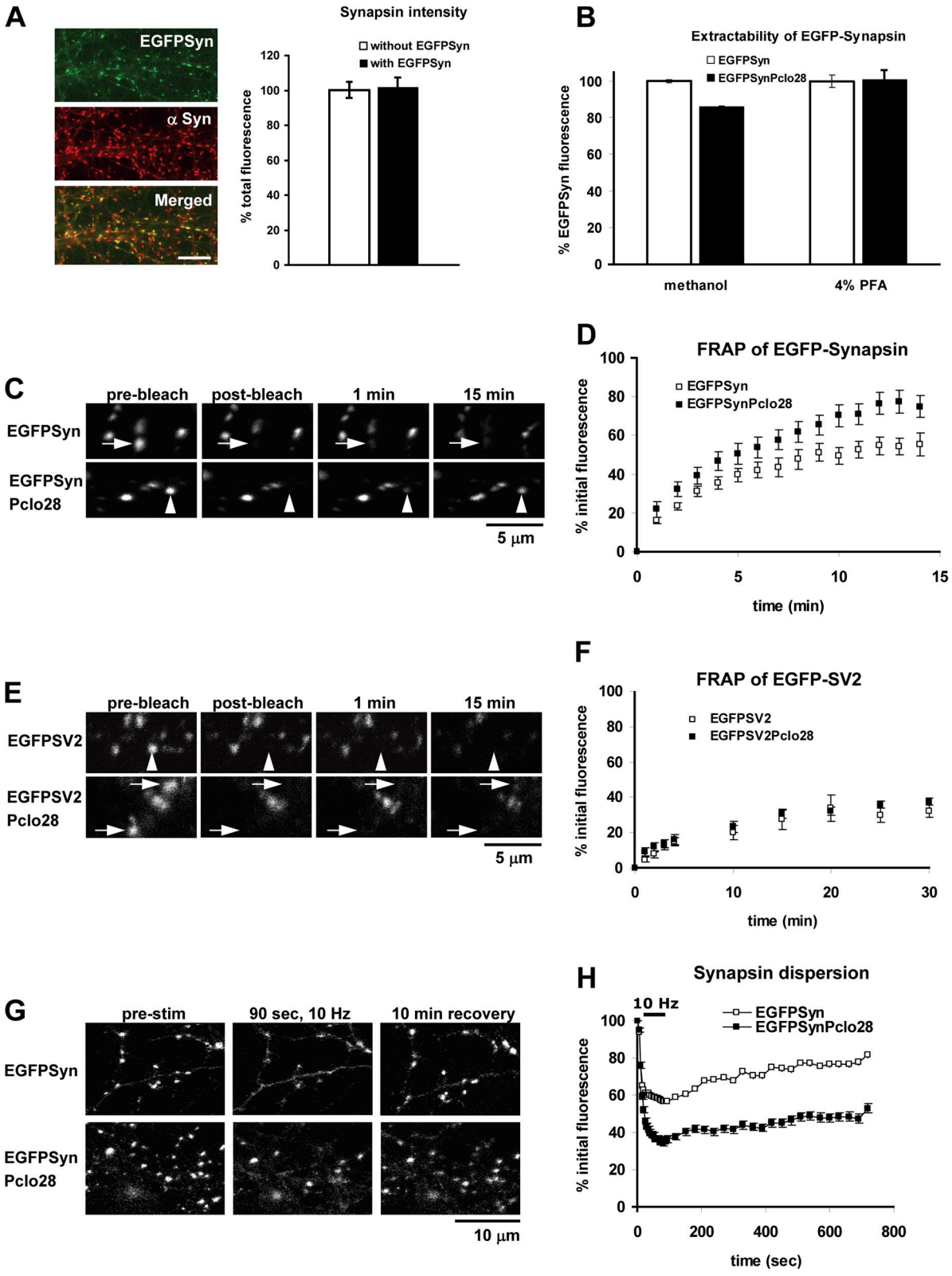

Figure 5. **Steady-state and activity-dependent dynamics of EGFP-Synapsin1a are altered at synapses lacking Piccolo.** (A, left) Images of neurons infected with EGFP-Synapsin1a (green) and immunostained with Synapsin1a antibodies (red). (A, right) Bar graph comparing the intensity of Synapsin immunoreactivity at boutons with or without EGFP-Synapsin1a. Total Synapsin levels are similar for infected and uninfected neurons. $n > 100$ puncta per condition. Bar, 10 μm. (B) EGFP-Synapsin1a fluorescence intensity at presynaptic boutons with (EGFPSyn) or without (EGFPSynPclo28) Piccolo after methanol versus 4% paraformaldehyde fixation ($n > 800$ puncta, seven fields of view per condition). (C) Time-lapse images of EGFP-Synapsin1a puncta. Single fluorescent puncta (indicated by arrows) were photobleached and their recovery was monitored over time. (D) Fluorescence recovery curves for EGFP-Synapsin1a puncta at boutons with (EGFPSyn, $n = 20$) or without (EGFPSynPclo28, $n = 17$) Piccolo. (E) Images of EGFP-SV2 puncta at boutons with (EGFPSV2) or without (EGFPSV2Pclo28) Piccolo, photobleached as in C. Arrowheads indicate the positions of EGFP puncta that are bleached during FRAP experiments.

http://www.jcb.org/cgi/content/full/jcb.200711167/DC1). However, in contrast to Synapsin1a, the exchange kinetics of EGFP-SV2 were not altered in the absence of Piccolo (Fig. 5, E and F). These data indicate that general presynaptic stability and SV retention were not significantly altered in the absence of Piccolo.

To assess whether the differences in steady-state exchange kinetics translated into activity-dependent differences in the dispersion kinetics of EGFP-Synapsin1a, we used an electrical stimulation protocol (10 Hz for 90 s) shown to promote the dispersion of Synapsin1a (Chi et al., 2001, 2003). Here, changes in the fluorescence intensity of EGFP-Synapsin1a at individual boutons were monitored both during stimulation and for the subsequent 10-min recovery period. In contrast to wild-type boutons, we observed both a more complete dispersion of EGFP-Synapsin1a and a slower rate of recovery in boutons lacking Piccolo (two-way ANOVA, $P < 0.0001$; Fig. 5, G and H). Intriguingly, we also observed remarkable, previously unreported heterogeneity in the extent of EGFP-Synapsin1a dispersion at individual boutons under both conditions. To evaluate whether the extent of EGFP-Synapsin1a dispersion was coupled to the rate of SV exocytosis, we simultaneously monitored the loss of EGFP-Synapsin1a and FM5-95 fluorescence from boutons during 5-Hz stimulation for 3 min. Our analysis revealed a tight correlation between the two events. At boutons with minimal EGFP-Synapsin dispersion (<10% for all time points), very little FM5-95 destaining occurred (Fig. 6, A and B). In contrast, synapses with more complete EGFP-Synapsin dispersion (>40% after 30 s of stimulation) exhibited dramatic FM5-95 destaining (Fig. 6, A and B). This feature was present both at control synapses (Fig. 6 A) and those lacking Piccolo (Fig. 6 B). A statistical analysis of the final fluorescence intensity values for EGFP-Synapsin and FM after the 3-min stimulation revealed a strong correlation between the extent of EGFP-Synapsin dispersion and that of FM5-95 destaining at both control boutons and those lacking Piccolo (control: $\rho = 0.58$, $P < 0.0001$; Pclo28: $\rho = 0.59$, $P < 0.0001$; Fig. 6, C and D). Although this tight correlation was observed for all synapses, the mean degree of Synapsin dispersion and FM destaining was greater at boutons lacking Piccolo, significantly shifting these correlation values to the lower right (Fig. 6, C and D). These data strongly indicate that the accelerated SV exocytosis rates observed at synapses lacking Piccolo are coupled to concomitant increases in the dispersion kinetics of Synapsin1a.

Changes in SV exocytosis and Synapsin dynamics are not observed at synapses lacking Bassoon

Piccolo shares a high degree of structural similarity with Bassoon (Fenster et al., 2000), another CAZ protein, and it is often assumed that these two proteins are functionally redundant (Fejtova and Gundelfinger, 2006; Schoch and Gundelfinger, 2006). We were thus interested in exploring whether the phenotypes seen at boutons lacking Piccolo were also observed in boutons lacking Bassoon. To this end, we generated a set of shRNAs against Bassoon and, after initial screening in the pZOff vector (unpublished data), subcloned one (Bsn16) into the LV/EGFP-Synapsin1a vector under the control of the H1 promoter. This shRNA was found to efficiently and specifically reduce the expression of Bassoon in lysates of cultures infected with LV/EGFP-Synapsin1a/Bsn16 on the day of plating and were harvested after 14 DIV (Fig. 7 A). Similarly, at the synaptic level, we observed a dramatic decrease (>95%) in the percent colocalization of Bassoon and EGFP-Synapsin1a in axons along dendritic profiles (Fig. 7, B and D). This decrease was not observed for Piccolo (Fig. 7, C and E), which indicates that the Bsn16 shRNA is specific for Bassoon.

We next examined whether boutons lacking Bassoon also exhibited changes in the dispersion and reclustering rates of EGFP-Synapsin1a. As shown in Fig. 7, synapses lacking Bassoon exhibited no detectable defects in EGFP-Synapsin dispersal or reclustering (Fig. 7 F) and no change in the destaining kinetics of FM5-95 (Fig. 7 G). Together, these observations strongly argue that the phenotypes observed for Piccolo are real and not artifacts of long-term shRNA expression. Moreover, they indicate that sequence elements unique to Piccolo play a fundamental role in negatively regulating SV exocytosis, apparently by influencing the activity-dependent dispersion of Synapsin1a.

Loss of Piccolo enhances the CaMKII sensitivity of Synapsin 1a

Because the association of Synapsin1a with SVs and the actin cytoskeleton in nerve terminals appears to be regulated by CaMKII phosphorylation (Schiebler et al., 1986; Benfenati et al., 1992; Greengard et al., 1993; Stefani et al., 1997; Chi et al., 2001, 2003), we next asked whether the altered dynamics of EGFP-Synapsin1a in the absence of Piccolo could be caused by changes in its CaMKII-dependent phosphorylation. This was examined by blocking CaMKII activity with 10 uM KN62 before and during a 10-Hz, 90-s stimulation. Surprisingly, KN62 had no significant effect on the dispersion kinetics or total amount of dispersion observed for EGFP-Synapsin in wild-type boutons (two-way ANOVA, $P = 0.15$; Fig. 8, A and C). However, it caused a dramatic reduction in EGFP-Synapsin dispersion at Pclo28 boutons, "rescuing" dispersion to levels seen at wild-type boutons (two-way ANOVA, $P < 0.0001$; Fig. 8, B and C). To determine whether this decrease in dispersion was accompanied by a decrease in the SV exocytosis rate, we also assessed the impact of KN62 on the destaining kinetics of FM5-95 at Pclo28 boutons. Again, KN62 attenuated the Pclo28 phenotype, slowing the accelerated exocytosis of SVs seen in the absence of Piccolo (two-way ANOVA, $P < 0.0001$; Fig. 8 D). These results indicate that the effects of Piccolo on presynaptic function are

(F) Fluorescence recovery curves for EGFP-SV2 puncta at synapses with (EGFPSV2, $n = 8$) or without (EGFP-SV2Pclo28, $n = 12$) Piccolo. (G) Time-lapse images of EGFP-Synapsin1a puncta. Images were acquired before, during, and after Synapsin dispersion was elicited with 10-Hz, 90-s stimulation. Shown here are sample images taken before and immediately after stimulation (10 Hz for 90 s) as well as after 10 min of recovery. (H) Graphical representation of data from G plotting the mean change in fluorescence intensity over time at boutons with or without Piccolo ($n > 100$ puncta per condition). The bar in the top left indicates time during which stimulation (10 Hz) was applied. Error bars indicate SEM.

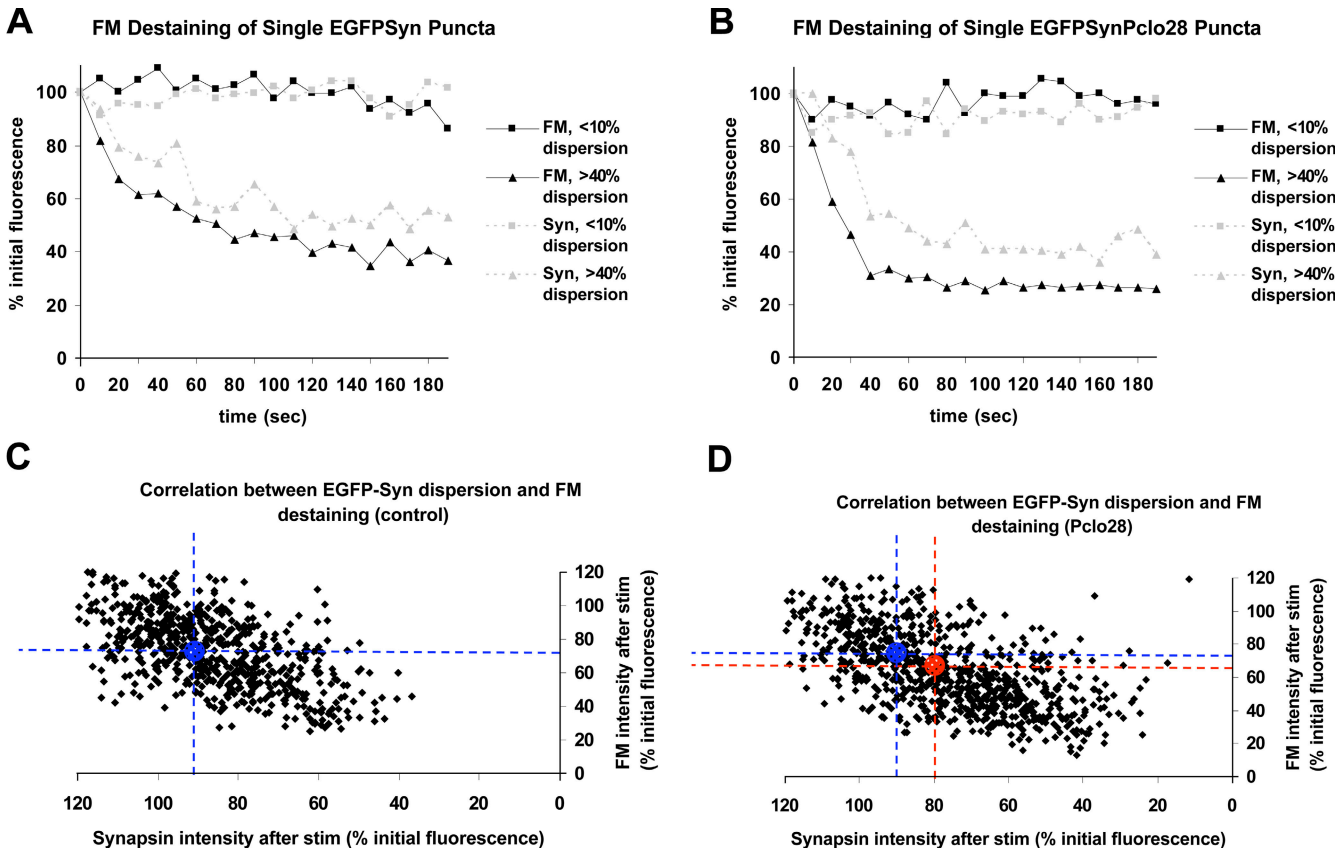

Figure 6. **Synapsin1a dispersion and FM destaining are tightly correlated.** (A and B) FM5-95 destaining curves for individual EGFP-Synapsin1a puncta at boutons with (A) or without (B) Piccolo. Shown in black are examples of FM destaining curves for which there was either dramatic (>40%; triangles) or minimal (<10%; squares) dispersion of Synapsin. Shown in light gray are EGFP-Synapsin intensities for these boutons. (C and D) Correlation analysis of EGFP-Synapsin1a dispersion and FM5-95 destaining at synapses with (C) or without (D) Piccolo. Plotted are EGFP-Synapsin1a and FM intensity values (expressed as a percentage initial fluorescence) at the final time point (t =180 s) of 5-Hz stimulation (control = 709 puncta; Pclo28 = 855 puncta). Dashed lines and circles indicate mean intensity values for Synapsin and FM at control boutons (blue; 90.8 ± 1.0% and 75.6 ± 0.9%, respectively) and those lacking Piccolo (red; 79.2 ± 0.9% and 65.5 ± 0.8%, respectively). Note that values for boutons lacking Piccolo are significantly shifted toward the bottom right.

mediated by CaMKII. Moreover, they provide further evidence that the Synapsin dispersion and SV exocytosis phenotypes are mechanistically linked.

Synapsin1a is hypophosphorylated in the absence of Piccolo

The ability of KN62 to rescue the Pclo28 phenotypes suggested that Synapsin might be hyperphosphorylated by CaMKII in the absence of Piccolo. To test this idea, we probed Western blots of hippocampal lysates containing (EGFPSyn) or lacking (Pclo28) Piccolo with two phospho-Synapsin1a antibodies that recognize sites phosphorylated by CaMKII or MAPK (Fig. 9 A; Chi et al., 2003). In these experiments, lysates from 14-DIV cultures were analyzed either directly (untreated) or after high-K+ treatment (90 mM KCl for 2 min) to stimulate Synapsin phosphorylation. As expected, the levels of both endogenous and EGFP-Synapsin1a phosphorylation at sites 3, 4, and 5 increased in all lysates after high-K+ stimulation (Fig. 9 B). However, in lysates from Pclo28 neurons, the levels of phosphorylation at these sites under both basal and high-K+ conditions were dramatically reduced (Fig. 9 B). This unexpected finding suggested that the kinase/phosphatase balance at boutons lacking Piccolo was altered and that perhaps these boutons exhibited enhanced phosphatase activity. To test this hypothesis, we screened a panel of phospho-specific antibodies against several pre- and postsynaptic proteins, including GluR1, Synaptotagmin, Rabphilin, Munc18, and Dynamin. Intriguingly, the phosphorylation levels of these proteins as assessed by Western blotting were not altered in the absence of Piccolo (Fig. 9 C), which indicates that the effect could be specific to Synapsin.

Discussion

In the present study, we have used interference RNAs to disrupt expression of the AZ protein Piccolo in developing hippocampal neurons. This knockdown was specific for Piccolo and had no overt effects on the expression or synaptic localization of other pre- and postsynaptic proteins, including Bassoon, Synapsin, Synaptophysin, RIM1α, Munc13, PSD-95, and NR1, or on the differentiation or life span (>4 wk) of cultured hippocampal neurons. Furthermore, we detected no gross changes in the size or morphology of excitatory glutamatergic synapses formed in the absence of Piccolo, which indicates that Piccolo is not essential for their assembly. Using live-imaging techniques, we also assessed a possible role for Piccolo in presynaptic function. We found that synapses lacking Piccolo were active and capable of

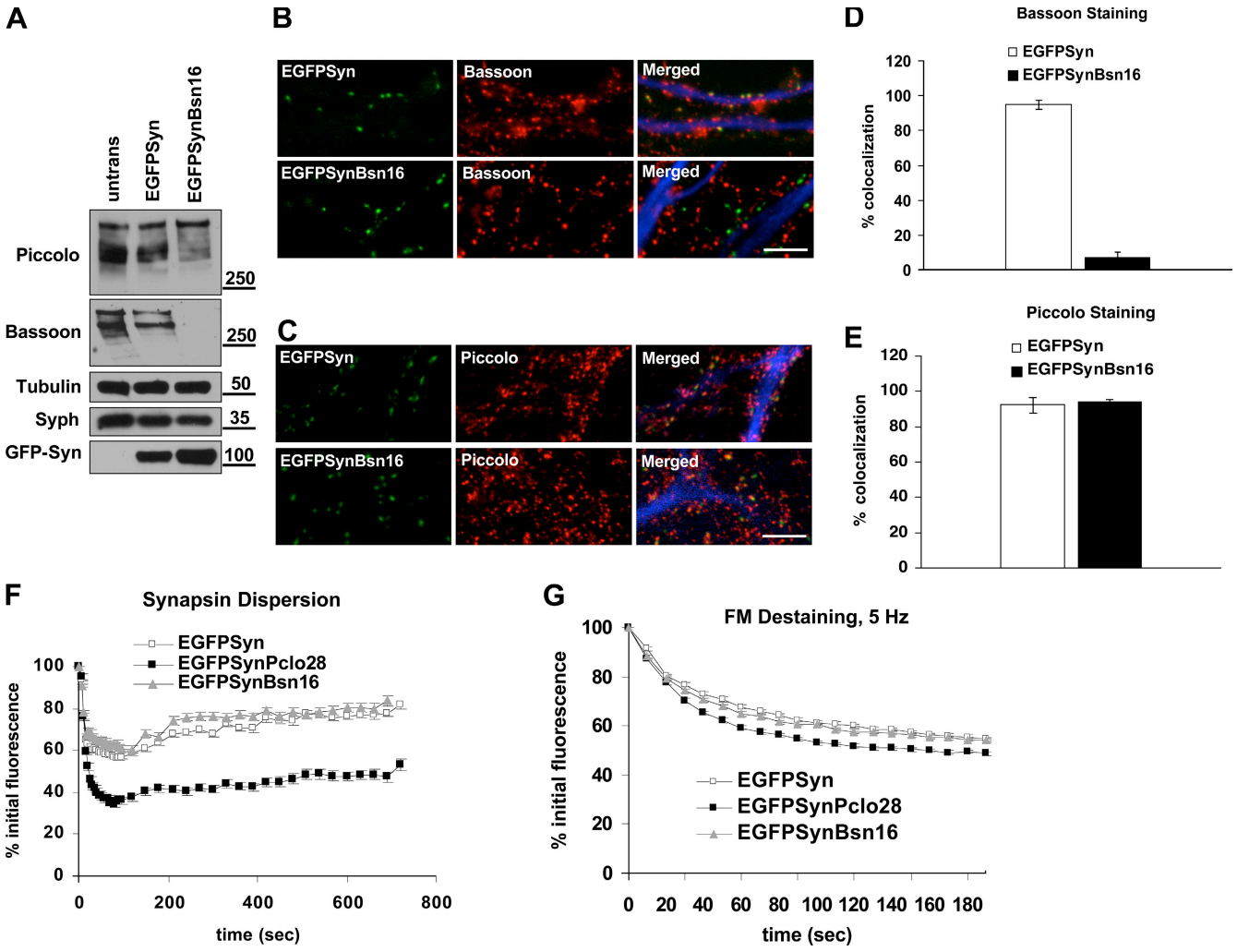

Figure 7. **Synapsin1a dispersal and SV exocytosis are normal in synapses lacking Bassoon.** (A) Western blots of lysates from neurons infected with LV/EGFP-Synapsin1a or LV/EGFP-Synapsin1a/Bsn16 and immunostained with antibodies against Piccolo, Bassoon, Synaptophysin (Syph), β-tubulin, or EGFP after 14 DIV. Protein molecular weights are indicated on the right. (B and C) Images of hippocampal neurons infected with LV/EGFP-Synapsin1a or LV/EGFP-Synapsin1a/Bsn16 and immunostained with antibodies against MAP2 (blue), Bassoon (B, red), or Piccolo (C, red). Bars, 10 µm. (D and E) Bar graphs quantifying the percent colocalization of Bassoon (D) or Piccolo (E) immunoreactive puncta with EGFP-Synapsin1a clusters along dendritic profiles. (F) Dispersion and reclustering kinetics of EGFP-Synapsin1a in control boutons (EGFPSyn) and those lacking Piccolo (EGFPSynPclo28) or Bassoon (EGFPSynBsn16). EGFPSyn and EGFPSynPclo28 curves are from Fig. 5 H (n = ∼100 puncta per condition). Error bars indicate SEM. (G) Destaining kinetics of FM5-95 during 5-Hz stimulation for control boutons (EGFPSyn) and those lacking Piccolo (EGFPSynPclo28) or Bassoon (EGFPSynBsn16). *n* > 200 puncta, two experiments per condition. Error bars indicate SEM.

recycling FM dyes but exhibited enhanced rates of SV exocytosis. Mechanistically, this phenotype was not caused by changes in the size or release probability of the RRP of SVs but rather to an increased dispersion of Synapsin1a from presynaptic boutons. This dispersion defect could be rescued by inhibiting CaMKII activity but was not caused by hyperphosphorylation of known Synapsin1a phospho sites by CaMKII. Importantly, synapses lacking Bassoon did not share these features. Together, these data indicate that Piccolo negatively regulates SV exocytosis by modulating Synapsin dynamics, thus potentially coupling the mobilization of SVs in the reserve pool to events at the AZ.

Roles of CAZ proteins at presynaptic boutons

So far, loss of function studies on CAZ proteins have primarily demonstrated defects in SV docking, priming, and fusion, as seen for Munc18, Munc13, and Rim1α (Augustin et al., 1999; Verhage et al., 2000; Schoch et al., 2002; Weimer and Richmond, 2005; Schoch and Gundelfinger, 2006). At present, it is unclear whether Piccolo and Bassoon are involved in these processes. Their high structural similarity and near-complete overlap of binding partners (Wang et al., 1999; Fenster et al., 2000, 2003; Kim et al., 2003; tom Dieck et al., 2005; Fejtova and Gundelfinger, 2006), and thus likely functional redundancy, will make this issue difficult to resolve until the analysis of synapses lacking both proteins is possible.

However, studies of synapses lacking either Piccolo or Bassoon are beginning to reveal unique roles for each. For example, studies of photoreceptor ribbon synapses demonstrate a crucial functional role for Bassoon in the attachment of ribbons to the arciform density and in neurotransmission at these synapses (Altrock et al., 2003; Dick et al., 2003; tom Dieck et al., 2005).

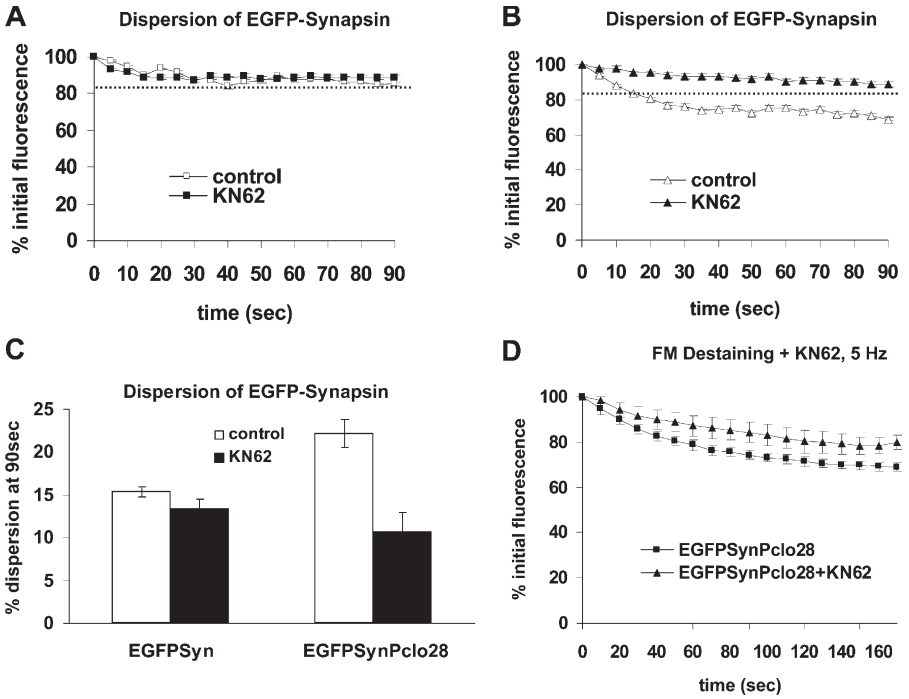

Figure 8. **CaMKII inhibition rescues the Pclo28 phenotypes.** (A) Dispersion kinetics of Synapsin1a in wild-type neurons incubated with (KN62) or without (control) 10 µM KN62 during a 90-s, 10-Hz stimulation. The broken gray line indicates maximal amount of dispersion (expressed as a percentage of initial fluorescence intensity before stimulation) seen in these neurons without KN62 (n > 100 puncta/condition). (B) Dispersion kinetics of Synapsin1a in neurons lacking Piccolo and incubated with (KN62) or without (control) KN62 during a 90-s, 10-Hz stim. For comparison, the broken gray line indicating maximal amount of dispersion observed in wild-type neurons is included (n > 100 puncta per condition). (C) Bar graphs summarizing the percent dispersion of EGFP-Synapsin1a puncta at synapses with (EGFPSyn) or without (EGFPSynPclo28) Piccolo in the presence or absence of KN62. Percent dispersion (100 − the percentage initial fluorescence) was measured at 90 s after a 10-Hz, 90-s stimulation (n = 2 experiments, 905 puncta for control without KN62; three experiments, 1,070 puncta for control + KN62; seven experiments, 2,195 puncta for Pclo28 without KN62; eight experiments, 2,341 puncta for Pclo28 + KN62). (D) Destaining kinetics of FM5-95 at boutons lacking Piccolo in the presence (triangles) or absence (squares) of KN62, during a 5-Hz, 180-s (900 pulse) stimulation (n = 5 experiments, 1,134 puncta for Pclo28 without KN62; two experiments, 437 puncta for Pclo28 + KN62). Error bars indicate SEM.

Furthermore, the increase in number of presynaptically silent synapses in Bassoon-deficient hippocampal neurons (Altrock et al., 2003) argues for a potential role of Bassoon in key aspects of vesicle release, perhaps similar to Munc13, Munc18, and Rim1α (Weimer and Richmond, 2005; Schoch and Gundelfinger, 2006). In contrast, we found no evidence that loss of Piccolo had any affect on the fraction of presynaptically silent synapses or on the size or release probability of the RRP of SVs. These data indicate that Piccolo does not directly participate in SV docking, priming, or fusion. Instead, our data reveal that Piccolo but not Bassoon influences the translocation of SVs from the reserve pool to the RRP by regulating the dynamic properties of Synapsin1a. These findings suggest that Piccolo may perform an integrative function within presynaptic boutons, coupling SV docking and fusion to the mobilization/recruitment of SVs from the reserve pool to the AZ.

Changes in the rates of SV exocytosis can be linked to altered Synapsin dynamics

Synapsins are a well-characterized family of presynaptic phosphoproteins thought to regulate the translocation of SVs from the reserve to the RRP (De Camilli et al., 1990; Greengard et al., 1993; Hilfiker et al., 1999). This concept is supported by knockout studies showing that Synapsins are essential for maintaining the size of the reserve pool of SVs (Li et al., 1995; Ryan et al., 1996) and by dynamic imaging studies, including this one, demonstrating that they regulate SV exocytosis rates at a range of stimulus frequencies (Chi et al., 2001, 2003). Importantly, the dynamic properties of Synapsin, particularly its activity-dependent dissociation from SVs and the actin cytoskeleton, are regulated by phosphorylation (Torri Tarelli et al., 1992; Hilfiker et al., 1999).

Although Synapsin is phosphorylated by multiple kinases, several studies have implicated CaMKII as its most prominent regulator (Schiebler et al., 1986; Benfenati et al., 1992; Ceccaldi et al., 1995; Stefani et al., 1997). However, these studies used in vitro binding assays, and none assessed the direct contribution of CaMKII to either the dispersion kinetics of Synapsin or to SV exocytosis in intact neurons. Two studies that did examine these functions used serine-to-alanine phospho mutants to demonstrate that the two identified CaMKII sites were important for regulating the rates of Synapsin dispersion and SV exocytosis (Chi et al., 2001, 2003). However, neither was performed at physiological temperatures and neither used pharmacological tools to assess the role of CaMKII in these processes.

In this study, we have carefully analyzed both the relationship between Synapsin dispersion and SV exocytosis, and the regulation of these events by CaMKII in intact neurons at physiological temperature. Regarding the former, our analysis of thousands of boutons revealed a remarkable and previously unreported heterogeneity in the degree of EGFP-Synapsin dispersion and FM5-95 destaining per bouton (from >50 to 0%). From this data, we observed a tight correlation between Synapsin dispersion and SV exocytosis. Though other studies have suggested such a relationship, ours is the first to conclusively demonstrate it. We have also closely examined the role of CaMKII in regulating Synapsin dispersion. Surprisingly, blocking

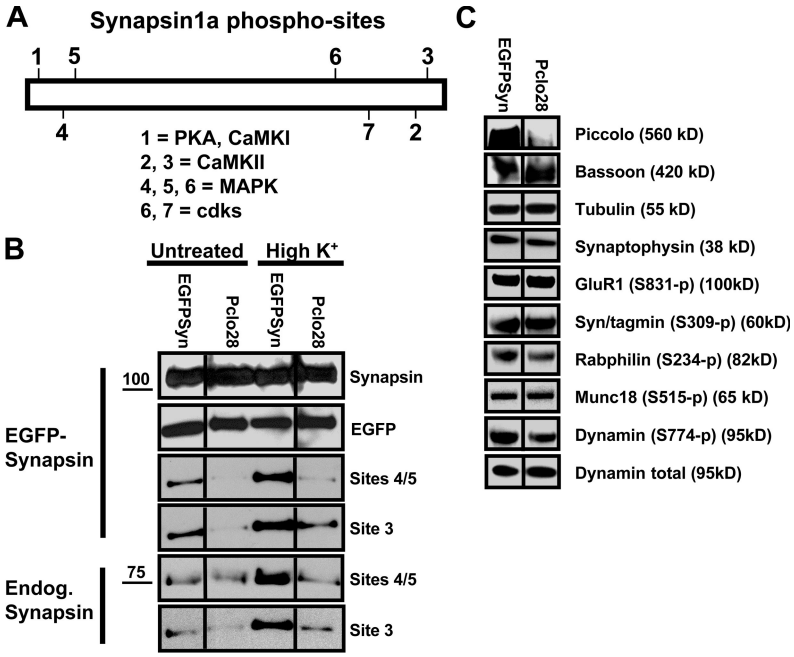

Figure 9. **Synapsin1a is hypophosphorylated in the absence of Piccolo.** (A) Schematic diagram of Synapsin1a illustrating the names and positions of each of its seven characterized phospho sites. (B) Western blot of hippocampal lysates from 14 DIV control cells (EGFPSyn) and those lacking Piccolo (Pclo28), untreated or treated with high K+ (2 min, 90 mM KCl) and probed with phospho-Synapsin antibodies recognizing site 3 or sites 4/5 as well as antibodies against total Synapsin1a and EGFP. (top) EGFP-Synapsin; (bottom) endogenous Synapsin. This experiment was repeated three times to verify the results. (C) Western blot of lysates from unstimulated control cells (EGFPSyn) and those lacking Piccolo (Pclo28) probed with antibodies against Piccolo, tubulin, Synaptophysin, and Dynamin, as well as phospho antibodies against GluR1, Synaptotagmin, Rabphilin, Munc18, and Dynamin. This experiment was performed twice to verify the results.

CaMKII activity with KN62 did not alter Synapsin dispersion in wild-type neurons, which suggests that other kinases may mediate this activity. This concept is supported by several previous studies indicating that protein kinase A and MAPK are important regulators of Synapsin, modulating its association with SVs or actin, respectively, and, in the case of MAPK, mediating SV exocytosis via Synapsin phosphorylation (Jovanovic et al., 1996; Hosaka et al., 1999; Jovanovic et al., 2000, 2001). Intriguingly, removing Piccolo from synapses caused Synapsin dispersion to be regulated by CaMKII. Furthermore, under these conditions, the enhanced rate of SV exocytosis was also CaMKII dependent, as both phenotypes could be rescued by inhibiting CaMKII with KN62. These data support our general conclusion that Piccolo negatively regulates SV exocytosis, apparently via a CaMKII-mediated mechanism.

We have also examined the phosphorylation state of Synapsin in the absence of Piccolo. We found that under basal conditions, Synapsin was hypophosphorylated at both CaMKII and MAPK sites. Although the levels of phosphorylation at both sites increased during stimulation, absolute levels of phosphorylation were always below those found in wild-type neurons. This finding was unexpected, as we had predicted based on multiple previous studies and our own experiments with KN62 that hyperphosphorylation of Synapsin would mediate its enhanced dispersion. However, total phosphorylation levels of Synapsin may not be predictive of its dispersion kinetics, as two other imaging studies have demonstrated that Synapsin dynamics are regulated through a complex combinatorial code of phosphorylation and dephosphorylation at its seven phospho sites (Chi et al., 2001, 2003). Furthermore, given Piccolo's putative role as a molecular organizer of the AZ, multiple signaling pathways may be subtly altered in its absence, affecting the balance of presynaptic phosphorylation/dephosphorylation in ways that are difficult to detect or interpret. In such a scenario, Synapsin would likely be one of many phospho proteins indirectly affected by the loss of Piccolo. However, if Synapsin dynamics/phosphorylation alone are altered (still a possibility given the lack of other detectable phenotypes), this would provide evidence for a more direct Piccolo–Synapsin interaction, perhaps through one of the actin-regulating proteins (ie. GIT1, Abp1, and profilin) known to bind Piccolo.

In conclusion, we have found that Piccolo is not essential for excitatory synapse formation but is a negative regulator of SV exocytosis. These results indicate that one of Piccolo's functions at the AZ is to regulate the translocation of SVs from the reserve to the RRP through modulation of Synapsin dynamics. Furthermore, our results demonstrate that this role is not shared by Bassoon, providing one of the first indications that these proteins have nonoverlapping functions. Rather puzzling is the absence of other presynaptic phenotypes, especially given the large size of Piccolo and its numerous binding partners. One likely explanation is that many of these are masked by redundant features in Bassoon, issues that will hopefully be resolved by the characterization of synapses lacking both Piccolo and Bassoon.

Materials and methods

Reagents

Antibodies against Piccolo (rabbit), Bassoon (mouse), and MAP2 (rabbit and mouse) were used as described previously (Zhai et al., 2000). HRP antibody was obtained from Advanced ImmunoChemical, Inc., GFP antibody from Roche, neomycin antibody from GeneTex, Inc., α-tubulin antibodies from Sigma-Aldrich, RIM1α and Munc13 from Synaptic Systems GmbH, PSD-95 from Affinity BioReagents, and NR1 from Millipore. Synaptophysin and Synapsin1 antibodies were obtained from Assay Designs and all phospho antibodies were obtained from PhosphoSolutions. Alexa 488 and 568 and Marina blue secondary antibodies were obtained from Invitrogen. Unless otherwise indicated, all other chemicals were obtained from Sigma-Aldrich.

Generation of pZOff vector

The pZOff vector was built on the backbone of the pEGFP-C1 vector (Clontech Laboratories, Inc.). Modifications include eliminating the multiple cloning site by digesting with BglII and BamHI and religating the vector. SalI, PvuI, and

BamHI restriction sites were subsequently inserted between the MluI and DraIII sites using oligos (5′-CGCGGTCGACGCGATCGCGGATCCTAC-3′ and 5′-GGATCCGCGATCGCGTCGAC-3′) that destroy both of these sites. The H1 promoter taken from the pSuper plasmid (Oligoengine) was inserted into with SalI and BamHI sites of the modified pEGFP vector, creating pZOff.

Design of shRNAs

shRNAs were designed corresponding to the 21-mer target sites using Ambion criteria specifying oligo duplexes with 5′-AA overhangs. The target sequence of Pclo28 is 5′-AAGTGCTGTCTCCTCTGTTGT-3′ (nucleotides 640–660 of *Rattus norvegicus* Piccolo from GenBank/EMBL/DDBJ under accession no. NM_020098). The target sequence of Pclo6 is 5′-AAGGGCGCAGGGGCTGCCCAA-3′ (nucleotides 334–354 of Piccolo from GenBank/EMBL/DDBJ under accession no. NM_020098) The target sequence of Bsn16 is 5′-AACACCTGCACCCAGTGTCAC-3′ (nucleotides 652–673 of *R. norvegicus* Bassoon from GenBank/EMBL/DDBJ under accession no. NM_0191416). Sense and antisense oligodeoxynucleotides (Sigma-Aldrich) contained looped overhangs for BglII and Hind III. The following oligos were used: Pclo28 sense, 5′-GATCCCCGTGCTGTCTCCTCTGTTGTTTCAAGAGAACAACAGAGGAGACAGCACTTTTTGGAAA-3′; Pclo28 antisense, 5′-AGCTTTTCCAAAAAGTGCTGTCTCCTCTGTTGTTCTCTTGAAACAACAGAGGAGACAGCACGGG-3′; Bsn16 sense, 5′-GATCCCCCACCTGCACCCAGTGTCACTTCAAGAGAGTGACACTGGGTGCAGGTG-3′; and Bsn16 antisense, 5′-AGCTTTTCCAAAAACACCTGCACCCAGTGTCACTCTCTTGAAGTGACACTGGGTGCAGGTGGGG-3′. Also used were: scrambled sense, 5′-GATCCCCTTGAGCAGCTAGGCGACCATTCAAGAGATGGTCGCCTAGCTCAATTTTTGGAAA-3′; and scrambled antisense, 5′-AGCTTTTCCAAAAATTGAGCAGCTAGGCGACCATCTCTTGAATGGTCGCCTAGCTGCTCAAGGG-3′. 100 pmol of the respective strands were annealed in annealing buffer (100 mM potassium acetate, 30 mM Hepes-KOH, pH 7.4, and 2 mM magnesium acetate) using a Thermocycler (Bio-Rad Laboratories). The annealed cDNA duplexes were then phosphorylated using phage T4 polynucleotide kinase (New England Biolabs, Inc.) and ligated into the pZOff vector between the BglII and HindIII sites.

Generation of FUGW H1vector

Converting the FUGW vector (Lois et al., 2002) into the shRNA silencing vector FUGW H1 required several steps. First, the EcoR1 site was eliminated from the FUGW vector. An oligonucleotide was then introduced into Pac1, creating a multicloning site with the following restriction enzyme sites: 5′ PvuI, BsiwI, EcoRI, BstBI, and PacI. Subsequently, the H1 promoter region and different shRNA sequences from the pZOff vector were inserted into the EcoRI and BstBI sites, creating FUGW H1. EGFP-Synapsin1a (a gift of T. Ryan, Weill Medical College of Cornell University, New York, NY) was incorporated into FUGW H1 by removing the EGFP cassette with XbaI and inserting the EGFP-Synapsin1a sequences into the Xba1 site (proteins were subcloned out of the pZOff vector using the NheI–XbaI sites; NheI is compatible with XbaI).

Lentivirus production

Lentivirus was produced by transfecting a three-plasmid vector system comprising a shuttle plasmid (FUGW or FU[Syn-EGFP]W) and two packaging plasmids (pCMVΔ R8.9 and pHCMV VSVg) into HEK293T cells (grown in DME + 10% fetal bovine serum and penicillin/streptomycin) as described previously (Lois et al., 2002). In brief, transfections were conducted on confluent (90–100%) cell cultures with Lipofectamine 2000 (Invitrogen) using 22.5 µg of total DNA and 60 µl lipofectamine per 10 cm plate. 2 d after transfection, the virus-containing medium was collected, passed through a 0.45-µm filter to remove cell debris, and frozen at −80°C. The viral titer was determined by fluorescence analysis of infected HEK293T cells (infective units).

Hippocampal cultures

Hippocampal cultures were prepared using a modified Banker culture protocol (Banker and Goslin, 1998). In brief, hippocampi from embryonic (embryonic day 18 or 19) Sprague-Dawley rats were dissected out and dissociated in 0.05% trypsin (Invitrogen), and cells were plated at a density of 165/mm^2 on poly-L-lysine–coated coverslips (Carolina Biological Supply Company). 1 h after plating, coverslips were transferred in pairs to 60-mm dishes containing a glial feeder layer, where they were inverted (to maximize neuronal contact with secreted glial factors) and maintained in neurobasal medium containing B27 and GlutaMAX (all from Invitrogen).

Hippocampal transfection and lentivirus infection

Hippocampal neurons were transfected or infected with the pZOff plasmid or lentivirus at the time of plating (0 DIV), respectively. The pZOff plasmid was introduced by electroporation of cells in suspension, conducted in 0.4-cm Gene Pulser Cuvettes (Bio Rad Laboratories) using 4 × 10^6 cells in 500 µl of glia-conditioned media (10% FBS and 20 mM glucose in glutamine-free MEM) and 20 µg of plasmid. Lentiviral infection was conducted after coverslips were transferred into 60-mm dishes using 10 µl of virus per dish to infect 20–30% of cells (for imaging experiments) and 100 µl/dish to superinfect ∼100% of cells (for all biochemical experiments).

Immunohistochemistry

Hippocampal neuronal cultures, grown for 5–21 DIV, were fixed with either 4% formaldehyde in 1× PBS for 10 min or 100% ice-cold methanol for 20 min. Cells were then permeabilized with 0.25% Triton X-100 in 1× PBS for 5 min, washed in PBS, incubated in blocking solution (2% bovine serum albumin, 2% glycine, and 0.2% gelatin in 50 mM NH_4Cl) for 15 min at room temperature, and incubated overnight at 4°C with primary antibodies in blocking solution. Afterward, cells were rinsed three to four times in PBS, incubated for 1 h at room temperature with secondary antibodies in blocking solution, rinsed again three to four times in PBS followed by a final rinse in deionized water, dried, and mounted in Vectashield mounting solution (Vector Laboratories).

Fixed images were acquired using a microscope (Axiovert 200M; Carl Zeiss, Inc.) with 100× 1.3 NA or 40× 1.3 NA Plan Neofluar objectives (Carl Zeiss, Inc.). Fluorescence images were acquired with OpenLab software (at 1,344 × 1,022 resolution, 12 bits per pixel; PerkinElmer) with blue fluorescent protein, FITC, and Texas red filter sets (Chroma Technology Corp.) using a digital camera (ORCA-ER; Hamamatsu). Quantification of colocalization was performed manually, by determining the percentage of Piccolo or Bassoon puncta that colocalized along dendritic (MAP2 positive) profiles with EGFP-Synapsin puncta.

Western blotting

Immunoblots of cellular lysates were prepared from either transfected HEK293 or infected hippocampal neurons. Transient transfections of 60–70% confluent HEK 293T cell cultures were performed using Lipofectamine 2000 (Invitrogen) with 10 µg of DNA per 10-cm plate. Homogenates from cells expressing Pclo28 or Bsn16 shRNAs were prepared 48 h after transfection. In brief, cells were harvested into homogenization buffer (ice-cold 1× PBS supplemented with protease inhibitors [complete protease inhibitor tablet, EDTA free; Roche]), and then placed directly into loading buffer. Protein levels were standardized empirically using a neomycin antibody and several loading concentrations. After separation by SDS-PAGE, proteins were transferred to nitrocellulose membranes (GE Healthcare) and probed with primary and secondary antibodies in Western blotting solution (5% nonfat dry milk and 0.05% NP-40 in Tris-buffered saline). Protein bands were visualized by HRP chemiluminescence (PerkinElmer). For Western blots of hippocampal cultures, neurons from lentivirus-infected coverslips were harvested directly into loading buffer and the same procedure was followed. Here, protein levels were standardized using tubulin or GFP antibodies.

EM

The ultrastructural analysis of glutamatergic asymmetrical synapses was performed on dissociated cultures of hippocampal neurons transfected by electroporation at the time of plating with pZOff-VAMP2-HRP ± Pclo28 shRNA. Samples were fixed with 2.5% glutaraldehyde in 0.15 M cacodylate buffer for 1 h and processed as described previously (Micheva and Smith, 2005) with a few modifications. In brief, after fixation, neurons were incubated with 1 mg/ml DAB (Sigma-Aldrich) in 50 mM Tris, pH 7.5, for 10 min. 0.01% H_2O_2 (Sigma-Aldrich) was then added to the DAB solution for 30 min at room temperature to stimulate HRP-mediated DAB precipitation. After extensive washing, neurons were prepared for EM by a microwave irradiation protocol described in detail previously (Micheva et al., 2003). After infiltration in Embed 812 (Electron Microscopy Sciences), glass coverslips were removed by dissolution in hydrofloric acid. Ultrathin 60-nm sections were cut with an ultramicrotome (Ultracut UCT; Leica) and placed on copper grids. Samples were poststained with 5% uranyl acetate dissolved in ultrapure water for 15 min followed by 4 min of staining in 0.2% lead citrate. Grids were extensively rinsed in water during and after poststaining. For control experiments (poststain No. 1 in Fig. S2), grids were more lightly poststained with 3.5% uranyl acetate in 50% acetone for 15 s followed by a 4-min 0.2% lead citrate stain. Samples were imaged with a transmission electron microscope (JEM-1230; JEOL Ltd.) at 80 kV accelerated voltage using a charge-coupled device camera (791; Gatan). All sample processing and EM was performed in the Cell Sciences Imaging Facility at Stanford University.

In a blinded fashion, control VAMP2-HRP and VAMP2-HRP-Pclo28 samples were imaged and synapses were quantitatively evaluated. Only

synapses with a clearly discernable PSD and at least two unambiguously HRP-labeled SVs were included in the analysis. The AZ was defined as the length of presynaptic membrane precisely opposed to the PSD. Docked SVs were defined as all SVs that had an edge within 25 nm of the AZ. All transmission EM quantitative analysis was performed using Image J.

Imaging experiments

All live imaging experiments were performed on a custom-built (by S. Smith, Stanford University, Stanford, CA; and N. Ziv, Technion Faculty of Medicine, Haifa, Israel) scanning confocal microscope (Axiovert 100TV; Carl Zeiss, Inc.) equipped with a 40× 1.3 NA Plan Neofluar objective (Car Zeiss, Inc.) and 488 nm and 514 nm lasers (Sapphire 488-20CDRH and Compass 215M-20; Coherent), using OpenView software (written by N. Ziv). Neuronal coverslips were mounted in a custom-built chamber designed for perfusion and electrical stimulation, heated to 37°C by a forced-air blower, and perfused with Tyrode's saline solution (25 mM Hepes, 119 mM NaCl, 2.5 mM KCl, 30 mM glucose, 2 mM CaCl, 2 mM $MgCl_2$, 50 µM CNQX, and 10 µM APV, pH 7.4).

FM loading/destaining

Functional presynaptic boutons were labeled with FM4-64 or FM5-95 dye (Invitrogen) by incubation in high-K+ Tyrodes solution (90 mM KCl and 31.5 mM NaCl) containing ~1 µg/ml FM dye for 60 s followed by normal Tyrodes + FM dye for 30 s. Neurons were then washed for ~5 min before imaging. Destaining was performed by electrical stimulation at the frequency (10, 5, or 2 Hz) and time interval (180, 90, and 30 s) specified for each experiment or by high-K+ Tyrodes solution for 60 s.

Image analysis and quantification were performed with OpenView software and Excel (Microsoft). GraphPad Prism (GraphPad Software) was used for statistical analysis. To measure the percentage of FM colocalization with EGFP-Synapsin clusters, the number of FM-containing clusters was divided by the total number of EGFP-Synapsin clusters and multiplied by 100. To calculate relative FM intensities at boutons containing or lacking Piccolo, FM intensity values for infected neurons were normalized against those from neighboring uninfected neurons in the same field of view, enabling cross-coverslip comparisons.

For FM destaining experiments at 5 and 10 Hz, the total number of action potentials elicited and images acquired were kept constant. Thus, at 10-Hz stimulation, images were acquired every 5 s for a total of 90 s, whereas at 5 Hz they were acquired every 10 s for a total of 180 s. In all cases, intensity values for a given FM punctum at each time point were expressed as a percentage of its initial fluorescence intensity before destaining using the following equation: (current FM intensity at time point *t*/initial FM intensity) × 100. For each condition (EGFPSyn and EGFPSynPclo28), intensity curves that did not exhibit FM destaining (ie. values >90% for all time points) were eliminated from the analysis. Remaining curves were pooled, averaged, and plotted using Excel.

Calculation of RRP size and Pr

Boutons were loaded using high-K+ Tyrodes to label the TRP (TRP label). RRP release was induced with either 500 mM sucrose or low-frequency electrical stimulation (2 Hz at 30 s; RRP release). Total FM destaining was induced with high-K+ stimulation for 60 s (background). To calculated RRP size, puncta intensity values were put into the following equation to express the RRP as a percentage of the TRP: {[(TRP label – background) – (RRP release – background)]/(TRP label – background)} × 100. Similar values were obtained for both methods, indicating that they can be used interchangeably to measure RRP.

To calculate Pr, the TRP was loaded with FM5-95 using high-K+ Tyrodes, and release of the RRP was induced using 2-Hz, 30-s electrical stimulation. During stimulation, images were acquired every 5 s. Intensity values were expressed as a percentage of initial fluorescence intensity, those exhibiting minimal destaining (values >95% for all time points) were eliminated from the analysis, and remaining curves were averaged and plotted as described in the previous section.

FRAP analysis

EGFP-Synapsin or SV2 puncta were bleached to ~20% of their initial fluorescence by a high-intensity laser beam (488 nm wavelength) at high magnification. Images were taken at a rate of 1 per minute to monitor fluorescence recovery for Synapsin, and 1 per minute followed by 1 per 5 minutes for SV2. For each time point, intensity values were expressed as a percentage of starting fluorescence before bleaching. To control for nonspecific photobleaching during image acquisition, the intensities of bleached puncta were normalized against those of unbleached puncta for each time point as described previously (Tsuriel et al., 2006), with the following equation: [(intensity of bleached Synapsin punctum at time *t*)/(mean intensity of all unbleached puncta in field of view at time *t*)] × 100. To control for variability in the extent of bleaching for each puncta, values were further normalized, making zero the default value for bleached puncta and enabling us to pool and average all recovery curves for a given condition (EGFPSyn and EGFPSynPclo28). τ values were calculated using a custom macro written in Excel (N. Ziv; Tsuriel et al., 2006).

Synapsin dispersion

Dispersion of EGFP-Synapsin was induced by electrical stimulation (10 Hz for 90 s) as described previously (Chi et al., 2001). Puncta intensity values were expressed as a percentage of initial fluorescence intensity before stimulation. Curves for all EGFP-Synapsin puncta were combined for a given condition (EGFPSyn and EGFPSynPclo28), averaged, and plotted. For this analysis, puncta that did not exhibit dispersion (percentage of initial fluorescence values > 90 for all time points) were excluded.

To compare extent of Synapsin dispersion to that of FM destaining, EGFP-Synapsin intensity was monitored during the 5-Hz destaining experiment (see FM destaining protocol).

To assess the role of CaMKII in Synapsin dispersion, coverslips were perfused with normal Tyrodes solution containing 10 uM KN62 (Tocris Bioscience) and incubated in the drug for 20 min before eliciting dispersion. EGFP-Synapsin intensity was monitored either before stimulation and every 5 s during stimulation (for dispersion curves), or before stimulation and at the last time point (t = 90 s; bar graphs).

FM5-95 destaining was also monitored after incubation with 10 µM KN62. For this experiment, boutons were first loaded with FM5-95 using high-K+ stimulation as described. After waiting 15 min to allow for some recovery of EGFP-Synapsin after stimulation, cells were incubated for an additional 20 min in 10 µM KN62. SV exocytosis was then elicited by 5-Hz stimulation for 180 s, and both FM intensity and EGFP-Synapsin intensity were monitored over this time period (images taken every 10 s). Destaining curves were then plotted as described and compared with destaining curves from untreated coverslips of cultures infected with LV/EGFP-Synapsin or LV/EGFP-Synapsin-Pclo28.

Online supplemental material

Fig. S1 shows initial testing of Piccolo shRNA (Pclo28) using pZOff plasmid-mediated knockdown in COS7 cells and neurons. Fig. S2 demonstrates that another shRNA against Piccolo (Pclo6) produces the same phenotypes as Pclo28. Fig. S3 shows additional EM micrographs showing that VAMP2-HRP unambiguously labels the synapses of transfected neurons and does not obscure synaptic junctions or other synaptic structures. Fig. S4 shows that EGFP-SV2, like EGFP-Synapsin, is a reliable presynaptic marker. Online supplemental material is available at http://www.jcb.org/cgi/content/full/jcb.200711167/DC1.

We are grateful to Noam Ziv, Nicole Calakos, and Rob Malenka for insightful suggestions and Tim Ryan for the EGFP-Synapsin clones. We also thank Kristina Micheva, John Perrino, and Yemane Gedde for their assistance with EM and hippocampal cultures.

This work was supported by grants from the National Institutes of Health (NS39471 and NS353862 to C.C. Garner), National Research Service Awards to C.L. Waites and R. Terry-Lorenzo, and the Bundesministerium für Bildung und Forschung to E.D. Gundelfinger.

Submitted: 30 November 2007
Accepted: 2 May 2008

References

Altrock, W.D., S. tom Dieck, M. Sokolov, A.C. Meyer, A. Sigler, C. Brakebusch, R. Fassler, K. Richter, T.M. Boeckers, H. Potschka, et al. 2003. Functional inactivation of a fraction of excitatory synapses in mice deficient for the active zone protein bassoon. *Neuron.* 37:787–800.

Augustin, I., C. Rosenmund, T.C. Sudhof, and N. Brose. 1999. Munc13-1 is essential for fusion competence of glutamatergic synaptic vesicles. *Nature.* 400:457–461.

Banker, G., and K. Goslin. 1998. Culturing Nerve Cells. Second edition. MIT Press, Cambridge, MA. 666 pp.

Benfenati, F., F. Valtorta, J.L. Rubenstein, F.S. Gorelick, P. Greengard, and A.J. Czernik. 1992. Synaptic vesicle-associated Ca2+/calmodulin-dependent protein kinase II is a binding protein for synapsin I. *Nature.* 359:417–420.

Cases-Langhoff, C., B. Voss, A.M. Garner, U. Appeltauer, K. Takei, S. Kindler, R.W. Veh, P. De Camilli, E.D. Gundelfinger, and C.C. Garner. 1996.

Piccolo, a novel 420 kDa protein associated with the presynaptic cytomatrix. *Eur. J. Cell Biol.* 69:214–223.

Ceccaldi, P.E., F. Grohovaz, F. Benfenati, E. Chieregatti, P. Greengard, and F. Valtorta. 1995. Dephosphorylated synapsin I anchors synaptic vesicles to actin cytoskeleton: an analysis by videomicroscopy. *J. Cell Biol.* 128:905–912.

Chi, P., P. Greengard, and T.A. Ryan. 2001. Synapsin dispersion and reclustering during synaptic activity. *Nat. Neurosci.* 4:1187–1193.

Chi, P., P. Greengard, and T.A. Ryan. 2003. Synaptic vesicle mobilization is regulated by distinct synapsin I phosphorylation pathways at different frequencies. *Neuron.* 38:69–78.

Cochilla, A.J., J.K. Angleson, and W.J. Betz. 1999. Monitoring secretory membrane with FM1-43 fluorescence. *Annu. Rev. Neurosci.* 22:1–10.

De Camilli, P., F. Benfenati, F. Valtorta, and P. Greengard. 1990. The synapsins. *Annu. Rev. Cell Biol.* 6:433–460.

Dick, O., S. tom Dieck, W.D. Altrock, J. Ammermuller, R. Weiler, C.C. Garner, E.D. Gundelfinger, and J.H. Brandstatter. 2003. The presynaptic active zone protein bassoon is essential for photoreceptor ribbon synapse formation in the retina. *Neuron.* 37:775–786.

Elferink, L.A., W.S. Trimble, and R.H. Scheller. 1989. Two vesicle-associated membrane protein genes are differentially expressed in the rat central nervous system. *J. Biol. Chem.* 264:11061–11064.

Fejtova, A., and E.D. Gundelfinger. 2006. Molecular organization and assembly of the presynaptic active zone of neurotransmitter release. *Results Probl. Cell Differ.* 43:49–68.

Fenster, S.D., and C.C. Garner. 2002. Gene structure and genetic localization of the PCLO gene encoding the presynaptic active zone protein Piccolo. *Int. J. Dev. Neurosci.* 20:161–171.

Fenster, S.D., W.J. Chung, R. Zhai, C. Cases-Langhoff, B. Voss, A.M. Garner, U. Kaempf, S. Kindler, E.D. Gundelfinger, and C.C. Garner. 2000. Piccolo, a presynaptic zinc finger protein structurally related to bassoon. *Neuron.* 25:203–214.

Fenster, S.D., M.M. Kessels, B. Qualmann, W.J. Chung, J. Nash, E.D. Gundelfinger, and C.C. Garner. 2003. Interactions between Piccolo and the actin/dynamin-binding protein Abp1 link vesicle endocytosis to presynaptic active zones. *J. Biol. Chem.* 278:20268–20277.

Friedman, H.V., T. Bresler, C.C. Garner, and N.E. Ziv. 2000. Assembly of new individual excitatory synapses: time course and temporal order of synaptic molecule recruitment. *Neuron.* 27:57–69.

Garner, C.C., S. Kindler, and E.D. Gundelfinger. 2000. Molecular determinants of presynaptic active zones. *Curr. Opin. Neurobiol.* 10:321–327.

Gracheva, E.O., A.O. Burdina, A.M. Holgado, M. Berthelot-Grosjean, B.D. Ackley, G. Hadwiger, M.L. Nonet, R.M. Weimer, and J.E. Richmond. 2006. Tomosyn inhibits synaptic vesicle priming in *Caenorhabditis elegans*. *PLoS Biol.* 4:e261.

Greengard, P., F. Valtorta, A.J. Czernik, and F. Benfenati. 1993. Synaptic vesicle phosphoproteins and regulation of synaptic function. *Science.* 259:780–785.

Hilfiker, S., V.A. Pieribone, A.J. Czernik, H.T. Kao, G.J. Augustine, and P. Greengard. 1999. Synapsins as regulators of neurotransmitter release. *Philos. Trans. R. Soc. Lond. B Biol. Sci.* 354:269–279.

Hosaka, M., R.E. Hammer, and T.C. Sudhof. 1999. A phospho-switch controls the dynamic association of synapsins with synaptic vesicles. *Neuron.* 24:377–387.

Jovanovic, J.N., F. Benfenati, Y.L. Siow, T.S. Sihra, J.S. Sanghera, S.L. Pelech, P. Greengard, and A.J. Czernik. 1996. Neurotrophins stimulate phosphorylation of synapsin I by MAP kinase and regulate synapsin I-actin interactions. *Proc. Natl. Acad. Sci. USA.* 93:3679–3683.

Jovanovic, J.N., A.J. Czernik, A.A. Fienberg, P. Greengard, and T.S. Sihra. 2000. Synapsins as mediators of BDNF-enhanced neurotransmitter release. *Nat. Neurosci.* 3:323–329.

Jovanovic, J.N., T.S. Sihra, A.C. Nairn, H.C. Hemmings Jr., P. Greengard, and A.J. Czernik. 2001. Opposing changes in phosphorylation of specific sites in synapsin I during Ca2+-dependent glutamate release in isolated nerve terminals. *J. Neurosci.* 21:7944–7953.

Kim, S., J. Ko, H. Shin, J.R. Lee, C. Lim, J.H. Han, W.D. Altrock, C.C. Garner, E.D. Gundelfinger, R.T. Premont, et al. 2003. The GIT family of proteins forms multimers and associates with the presynaptic cytomatrix protein Piccolo. *J. Biol. Chem.* 278:6291–6300.

Li, L., L.S. Chin, O. Shupliakov, L. Brodin, T.S. Sihra, O. Hvalby, V. Jensen, D. Zheng, J.O. McNamara, P. Greengard, et al. 1995. Impairment of synaptic vesicle clustering and of synaptic transmission, and increased seizure propensity, in synapsin I-deficient mice. *Proc. Natl. Acad. Sci. USA.* 92:9235–9239.

Lois, C., E.J. Hong, S. Pease, E.J. Brown, and D. Baltimore. 2002. Germline transmission and tissue-specific expression of transgenes delivered by lentiviral vectors. *Science.* 295:868–872.

Micheva, K.D., and S.J. Smith. 2005. Strong effects of subphysiological temperature on the function and plasticity of mammalian presynaptic terminals. *J. Neurosci.* 25:7481–7488.

Micheva, K.D., J. Buchanan, R.W. Holz, and S.J. Smith. 2003. Retrograde regulation of synaptic vesicle endocytosis and recycling. *Nat. Neurosci.* 6:925–932.

Mozhayeva, M.G., Y. Sara, X. Liu, and E.T. Kavalali. 2002. Development of vesicle pools during maturation of hippocampal synapses. *J. Neurosci.* 22:654–665.

Pyle, J.L., E.T. Kavalali, E.S. Piedras-Renteria, and R.W. Tsien. 2000. Rapid reuse of readily releasable pool vesicles at hippocampal synapses. *Neuron.* 28:221–231.

Ryan, T.A., H. Reuter, B. Wendland, F.E. Schweizer, R.W. Tsien, and S.J. Smith. 1993. The kinetics of synaptic vesicle recycling measured at single presynaptic boutons. *Neuron.* 11:713–724.

Ryan, T.A., L. Li, L.S. Chin, P. Greengard, and S.J. Smith. 1996. Synaptic vesicle recycling in synapsin I knock-out mice. *J. Cell Biol.* 134:1219–1227.

Sankaranarayanan, S., P.P. Atluri, and T.A. Ryan. 2003. Actin has a molecular scaffolding, not propulsive, role in presynaptic function. *Nat. Neurosci.* 6:127–135.

Schiebler, W., R. Jahn, J.P. Doucet, J. Rothlein, and P. Greengard. 1986. Characterization of synapsin I binding to small synaptic vesicles. *J. Biol. Chem.* 261:8383–8390.

Schoch, S., and E.D. Gundelfinger. 2006. Molecular organization of the presynaptic active zone. *Cell Tissue Res.* 326:379–391.

Schoch, S., P.E. Castillo, T. Jo, K. Mukherjee, M. Geppert, Y. Wang, F. Schmitz, R.C. Malenka, and T.C. Sudhof. 2002. RIM1alpha forms a protein scaffold for regulating neurotransmitter release at the active zone. *Nature.* 415:321–326.

Shapira, M., R.G. Zhai, T. Dresbach, T. Bresler, V.I. Torres, E.D. Gundelfinger, N.E. Ziv, and C.C. Garner. 2003. Unitary assembly of presynaptic active zones from Piccolo-Bassoon transport vesicles. *Neuron.* 38:237–252.

Stefani, G., F. Onofri, F. Valtorta, P. Vaccaro, P. Greengard, and F. Benfenati. 1997. Kinetic analysis of the phosphorylation-dependent interactions of synapsin I with rat brain synaptic vesicles. *J. Physiol.* 504:501–515.

Sudhof, T.C., M. Baumert, M.S. Perin, and R. Jahn. 1989. A synaptic vesicle membrane protein is conserved from mammals to *Drosophila*. *Neuron.* 2:1475–1481.

tom Dieck, S., L. Sanmarti-Vila, K. Langnaese, K. Richter, S. Kindler, A. Soyke, H. Wex, K.H. Smalla, U. Kampf, J.T. Franzer, et al. 1998. Bassoon, a novel zinc-finger CAG/glutamine-repeat protein selectively localized at the active zone of presynaptic nerve terminals. *J. Cell Biol.* 142:499–509.

tom Dieck, S., W.D. Altrock, M.M. Kessels, B. Qualmann, H. Regus, D. Brauner, A. Fejtova, O. Bracko, E.D. Gundelfinger, and J.H. Brandstatter. 2005. Molecular dissection of the photoreceptor ribbon synapse: physical interaction of Bassoon and RIBEYE is essential for the assembly of the ribbon complex. *J. Cell Biol.* 168:825–836.

Torri Tarelli, F., M. Bossi, R. Fesce, P. Greengard, and F. Valtorta. 1992. Synapsin I partially dissociates from synaptic vesicles during exocytosis induced by electrical stimulation. *Neuron.* 9:1143–1153.

Tsuriel, S., R. Geva, P. Zamorano, T. Dresbach, T. Boeckers, E.D. Gundelfinger, C.C. Garner, and N.E. Ziv. 2006. Local sharing as a predominant determinant of synaptic matrix molecular dynamics. *PLoS Biol.* 4:e271.

Verhage, M., A.S. Maia, J.J. Plomp, A.B. Brussaard, J.H. Heeroma, H. Vermeer, R.F. Toonen, R.E. Hammer, T.K. van den Berg, M. Missler, et al. 2000. Synaptic assembly of the brain in the absence of neurotransmitter secretion. *Science.* 287:864–869.

Waites, C.L., A.M. Craig, and C.C. Garner. 2005. Mechanisms of vertebrate synaptogenesis. *Annu. Rev. Neurosci.* 28:251–274.

Wang, X., M. Kibschull, M.M. Laue, B. Lichte, E. Petrasch-Parwez, and M.W. Kilimann. 1999. Aczonin, a 550-kD putative scaffolding protein of presynaptic active zones, shares homology regions with Rim and Bassoon and binds profilin. *J. Cell Biol.* 147:151–162.

Weimer, R.M., and J.E. Richmond. 2005. Synaptic vesicle docking: a putative role for the Munc18/Sec1 protein family. *Curr. Top. Dev. Biol.* 65:83–113.

Weimer, R.M., E.O. Gracheva, O. Meyrignac, K.G. Miller, J.E. Richmond, and J.L. Bessereau. 2006. UNC-13 and UNC-10/rim localize synaptic vesicles to specific membrane domains. *J. Neurosci.* 26:8040–8047.

Winter, C., S. tom Dieck, T.M. Boeckers, J. Bockmann, U. Kampf, L. Sanmarti-Vila, K. Langnaese, W. Altrock, M. Stumm, A. Soyke, et al. 1999. The presynaptic cytomatrix protein Bassoon: sequence and chromosomal localization of the human BSN gene. *Genomics.* 57:389–397.

Zhai, R., G. Olias, W.J. Chung, R.A. Lester, S. tom Dieck, K. Langnaese, M.R. Kreutz, S. Kindler, E.D. Gundelfinger, and C.C. Garner. 2000. Temporal appearance of the presynaptic cytomatrix protein bassoon during synaptogenesis. *Mol. Cell. Neurosci.* 15:417–428.

Zhai, R.G., H. Vardinon-Friedman, C. Cases-Langhoff, B. Becker, E.D. Gundelfinger, N.E. Ziv, and C.C. Garner. 2001. Assembling the presynaptic active zone: a characterization of an active one precursor vesicle. *Neuron.* 29:131–143.

Ziv, N.E., and C.C. Garner. 2004. Cellular and molecular mechanisms of presynaptic assembly. *Nat. Rev. Neurosci.* 5:385–399.